Carbonaceous aerosols in five European cities: Insights into primary emissions and secondary particle formation

Sarkawt Hama[a,b,c*], Ibrahim Ouchen[d], Kevin P. Wyche[e], Rebecca L. Cordell[a], Paul S. Monks*[a]

[a]*Department of Chemistry, University of Leicester, Leicester, LE1 7RH, UK*

[b]*Department of Chemistry, School of Science, University of Sulaimani, Sulaimani, Kurdistan region, Iraq*

[c]*Global Centre for Clean Air Research (GCARE), Department of Civil and Environmental Engineering, Faculty of Engineering and Physical Sciences, University of Surrey, Guildford, GU2 7XH, UK*

[d]*Earth Sciences Department, Scientific Institute, Mohammed V University, Rabat 10106, Morocco*

[e]*Centre for Earth Observation Science, School of Environment and Technology, University of Brighton, Brighton, BN2 4GJ, UK*

***Corresponding authors.** Email s.m.hama@surrey.ac.uk (Sarkawt Hama); paul.monks@leicester.ac.uk (Paul Monks)*

Graphical abstract

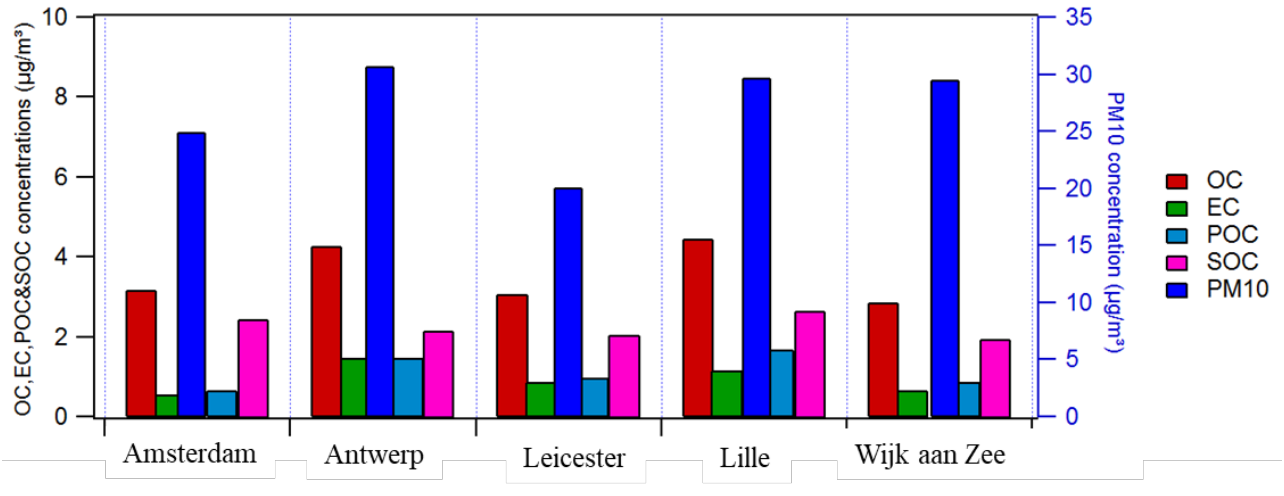

Abstract

Carbonaceous material is an important component of atmospheric aerosol particles, which plays a significant role in air quality and climate, and also has potentially negative impacts on human health. There is a lack of data reported in the literature regarding the carbonaceous fraction of aerosol in the North-West European 'air pollution hotspot' and this work reports a comprehensive one-year intensive measurement campaign, where organic carbon (OC) and elemental carbon (EC) fractions of PM_{10} (particulate matter of diameter ≤10 μm) were measured. Owing to the importance of carbonaceous aerosols in understanding particulate pollution sources, ~2,000 PM_{10} samples were simultaneously collected across North-West Europe at four urban background sites located in Amsterdam (AD), Antwerp (AP), Leicester (LE) and Lille (LL), and one industrial site at Wijk aan Zee (WZ). PM_{10} samples were chemically analysed by OC-EC analyser for carbonaceous species (OC, and EC) and trends were identified. OC accounted for 12.8%, 13.9%, 15.3%, 15.1% and 9.8%, and EC accounted for 2.4%, 4.9%, 4.4%, 4.0%, and 2.4% of total PM_{10} mass for AD, AP, LE, LL and WZ, respectively. Secondary organic carbon (SOC) contributions were higher in warmer months compared to colder months, and SOC concentration levels were similar at all five locations, with SOC contributing more than primary organic aerosol (POC) in each city. The lower effective carbon ratio (ECR) values (≤0.3) at all five sites in October, November, and February can be attributed to higher combined POC and EC concentrations and lesser contributions from SOC, meaning that SOC with a greater relative formation has a greater tendency to disperse solar radiation. Higher ECR values in April, May, and July, on the other hand, indicate that more absorbing types of carbonaceous aerosols are also present. More than 90% of the air-mass trajectories were from the north and northeast. This paper details atmospheric processes and sources influencing the seasonal variability of the carbonaceous components of PM_{10}.

Keywords: PM_{10}, chemical composition, seasonal variation, Elemental carbon, organic carbon, North-West Europe

Highlights:

- Carbonaceous aerosols concentrations have been measured in five cities across North-West Europe.
- Clear seasonal variation of OC/EC was observed with higher levels in winter/spring.
- Secondary organic aerosols (SOA) were the highest in spring at the five sites.
- SOA production is more affected by photochemistry than weather conditions.

1. Introduction

In the urban setting, atmospheric aerosols (often commonly referred to as particulate matter (PM)) derive from both natural and anthropogenic sources and primarily consist of a mixture of carbonaceous material, sulphates, nitrates, sea salts and mineral dust (WHO, 2016). Atmospheric PM has long been identified as a major air pollutant in urban areas (Hama et al., 2018; WHO, 2016; Harrison, 2020; Kelly and Fussell, 2015), both in terms of its impacts on the environment and on human health; indeed, PM is considered a significant risk factor in various negative human health endpoints on the global scale (WHO, 2016). PM can also directly influence climate by causing perturbation of the radiative balance of Earth's atmosphere through scattering and absorption of solar radiation (Ramana et al., 2010) and indirectly by acting as cloud condensation nuclei and changing cloud characteristics (Zhang, 2009). PM can also have negative impacts on visibility and ecosystems (Fan et al., 2012). Chemical composition is a significant factor in determining the ability of PM to impart these various impacts and as such chemical characterisation and source identification is paramount to advance our fundamental understanding and for the development of effective mitigation strategies and emissions reduction policies (Monks et al., 2009; Pöschl, 2005).

Atmospheric carbonaceous aerosols have drawn increasing attention in scientific research owing not only to their significant role in radiative forcing, visibility reduction and health and climate effects, but also because of the intricacies involved in deconvoluting their complex physicochemical properties (Bond et al., 2013; Janssen et al., 2011). Carbonaceous aerosols can make up a major fraction of atmospheric particulate matter mass concentrations, *i.e.* studies have shown that ~20–70% of total suspended particulate matter can be composed of carbonaceous matter in urban areas (Ramachandran et al., 2009). The carbonaceous fraction of ambient particles usually consists of organic carbon (OC) and elemental carbon (EC). OC can either be emitted directly from combustion processes and other sources (primary organic carbon; POC) or it can be formed in the atmosphere by oxidation reactions (secondary organic carbon; SOC) (Hallquist, et al., 2009). In urban areas, vehicle emissions are a significant source of POC, whereas SOC (is formed from the oxidation of both anthropogenic and biogenic volatile organic compounds (De Gouw and Jiménez, 2009) followed by nucleation/condensation processes including physical/chemical adsorption onto the surface of pre-existing particles (Fuzzi et al. 2006) EC is a primary pollutant emitted directly from fossil fuel combustion and biomass burning (IPCC, 2015). OC, which includes polycyclic aromatic

hydrocarbons (PAHs) and polychlorinated biphenyls, has been shown to be carcinogenic (Mauderly and Chow, 2008), while EC, which includes heavy metals and PAHs, can impart a range of other adverse effects on human health and environment (Biswas et al., 2009).

The temporal and spatial variability of OC and EC performed in recent study showed that the characteristics of carbonaceous aerosols are spatially similar and season dependent, in particular with the production of secondary organic aerosol (SOA) enhanced during autumn and winter (Cesari et al., 2018). In addition, the seasonal analysis of carbonaceous aerosols revealed the extent of some trends OC concentrations higher in summer and EC higher in winter (Cesari et al., 2018). The meteorological parameters (wind speed, and wind direction, boundary layer dynamic, ambient temperature, and relative humidity) have significant influences on the concentration of carbonaceous aerosol in the atmosphere (Sonwani et al., 2021; Saxena & Sonwani, 2019). Several studies have also mentioned the importance of meteorological conditions in OC and EC variations in the atmosphere (Kumar & Yadav, 2016; Sonwani et al., 2021). In addition, a study in India found that the carbonaceous components were substantially linked with rain intensity during pre-monsoon and monsoon seasons (Sonwani and Saxena, 2021; Sonwani et al., 2021). Another study revealed that the meteorological parameters such as temperature, wind direction, and atmospheric stability significantly affect the levels of OC as compared to that of EC during summer and winter seasons (Sonwani et al., 2021).

The north-western part of Europe is considered, a ‘hot-spot’ region for air pollution, with high outdoor concentrations of PM, ozone, sulfur dioxide and nitrogen oxides (Cordell et al., 2016; Hama et al., 2017a; EEA, 2019; Wyche et al., 2020). Current monitoring efforts generally focus on PM mass concentration in-line with current air quality legislation (2008/20/EC), but these data normally do not allow the assessment of various sources across the region. To enable the development of health-relevant air quality policies in North-West Europe (NW Europe) a better understanding of sources and composition of PM is required. Despite the very significant role of PM in climatic, environmental and health effects, our knowledge of aerosol chemical composition, particularly the carbonaceous fraction, is limited, particularly for PM in the North-West European hot-spot region. Indeed, currently, the sources, formation mechanisms and transformation processes of carbonations components of PM still remain to be comprehensively addressed well. As such, the main aim of this study is to better understand the spatio-temporal evolution of carbonaceous aerosols, and the formation of SOA in the urban background of North-West Europe. The study was carried out between April 2013 and May 2015 as part of the Joint Air Quality Initiative (JOAQUIN) project (Hofman et al., 2016; Hama

et al., 2017a, and 2017b), and involved the collection of PM_{10} samples at five different locations, including Amsterdam and Wijk aan Zee (the Netherlands); Antwerp (Belgium); Leicester (United Kingdom); and Lille (France). The samples were collected and analysed using a common approach in an effort to harmonise methodologies and improve incomparability.

2. Experimental

2.1 Monitoring sites

PM samples were collected at five sites in NW Europe: Amsterdam (AD); Wijk aan Zee (WZ); Antwerp (AP); Leicester (LE); and Lille (LL) (see Figure 1). The detailed site descriptions are summarised in Table 1. WZ is an industrial monitoring site of Province North Holland, located approximately 30 km west from Amsterdam. WZ site is located at the north side of a parking lot and it is used by visitors of a camping site (Banjaert). Residences of Wijk aan Zee inhabitants are present at a distance of approximately 40 m. The nearest road (Burgemeester Rothestraat) is at a distance of 70- 80 m to the south and west. The nearest main road (Verlengde Voorstraat) is at 175 m. The industrial zone of IJmond is located east (750 m) and south (1-2 km) of the site. The main activities in the industrial zone are the production of steel (Tata Steel, south of the site) and energy company which provides electricity and natural gas (previous name of the company was "NUON", current name is "Vattenfall Nederland B.V." (Joaquin, 2015). The four others are considered to be urban background sites for PM_{10} monitoring. Details about the characteristics and locations of the sampling sites can be found in Cordell et al. (2016). For a detailed overview of the sampling sites and the JOAQUIN project, refer to the final project report (Joaquin, 2015). High resolution meteorological data (Ambient air temperature (T), Relative Humidity (RH) and Air Pressure (P), Radiation (RAD) and precipitation (PREC)) for each site separately were acquired from nearest stations (Table S1). Figure S1 shows the monthly values of ambient temperature and relative humidity for each site to allow us to see the monthly variations in each monitoring station.

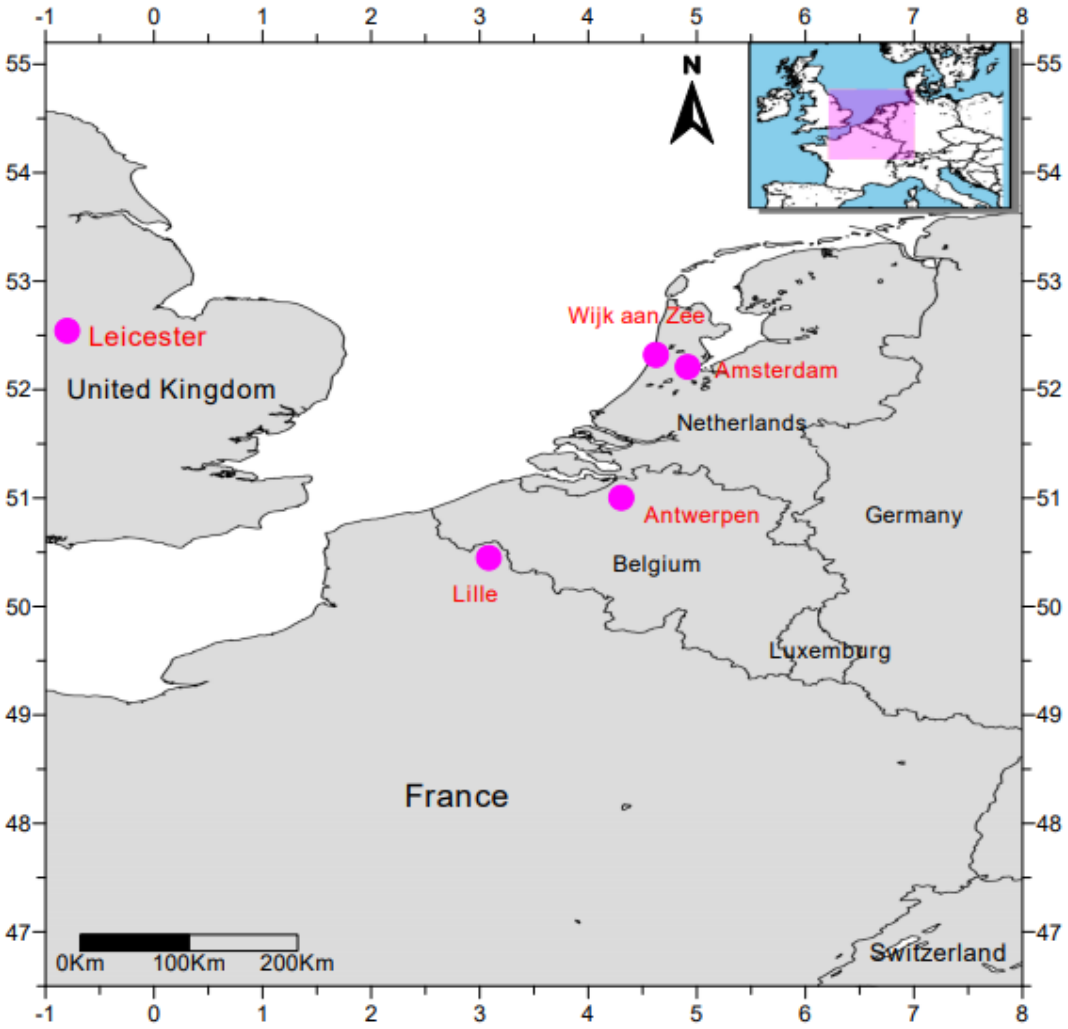

Figure 1. Location of monitoring sites: Amsterdam and Wijk aan Zee (the Netherlands); Antwerp (Belgium); Leicester (United Kingdom); and Lille (France).

Table 1. Details of location of monitoring sites. The symbol '-' shows the unavailability of the data.

City (code)	Site designation	Distance to main street (m)	Traffic intensity[a] vehicles day^{-1}	Coordinates Latitude/Longitude
Amsterdam (AD)	Urban Background	64	15,000[b]	52°21′35″ N/4°51′59″ E
Antwerp (AP)	Urban Background	30	29,500[c]	51°12′35″ N/4°25′55″ E

Leicester (LE)	Urban Background	140	22,500[d]	52°37′12″ N/1°07′38″ W
Lille (LL)	Urban Background	35	-	50° 37′ 41″ N/3° 05′ 25″ E
Wijk aan Zee (WZ)	Industrial	70	-	52° 49′ 40″ N/4° 60′ 23″ E

[a]Mean annual traffic intensity at the nearest main street; [b]Year 2015: (CoA, 2020); [c]Year 2013: (VMM, 2020); [d]Year 2013: (DfT, 2020).

2.2. Aerosol collection and Chemical analysis

PM_{10} samples were collected from April 2013 to May 2014, except for Lille where the measurements started two months later (June 2013 to May 2014). The collected number of filter samples for each monitoring site is summarised in Table S2. The samples were collected daily (24 h exposure) onto 47 mm quartz filters (Pall Tissuquartz™ filters, 2500 QAT-UP) using a sequential sampler (Derenda PNS16 (https://www.comde-derenda.com/wp-content/uploads/2016/10/db-221-en-PNS16T.pdf) in Amsterdam and Wijk aan Zee and Leckel SEQ47/50 (https://www.leckel.de/devices/seq4750-rv/) in Antwerp , Leicester and Lille, with a PM_{10} inlet running at 2.3 $m^3\ h^{-1}$. Flows were checked every 14 days when changing the filter compartments. PM_{10} samples that were collected every 6th day of the period were analysed for elemental and organic carbon. Filters were weighed before and after sampling in order to determine total PM_{10} mass collected. For pre- and post-sampling, filters were conditioned at 20 ± 1 °C and 50 ± 5% relative humidity for 48 h, weighed, left for a further 24 h and re-weighed. Both the real samples and the blank filters were weighed and the PM_{10} mass for the actual samples were corrected for the net masses obtained from the blank filters. After sampling, the filters were sealed in aluminium foil bags and stored in a freezer (-18 °C) prior to analysis. Six punches of 1 cm^2 were taken for chemical analysis using. Identical 1.0 cm × 1.0 cm punchers (SunSet Laboratory Inc., USA). One punch was employed to determine the elemental and organic carbon (EC/OC). OC and EC concentrations were determined using the OC-EC analyser (Model 5L, Sunset Laboratory Inc., USA), employing the NIOSH-870 (National Institute of Occupational Safety and Health) protocol based on thermal-optical transmittance (Joaquin, 2015, Panteliadis et al., 2015). The method detection limits (MDLs) values for OC and EC were 0.01 μg/m3, more details can be found in (Joaquien, 2015) and in Section S1 (Table S3). Further information regarding other chemical analyses and

quality control and assurance processes for the JOAQUIN project can be found in (Cordell et al., 2016; Joaquin, 2015; Cordell et al., 2014).

2.3 Estimation of secondary organic carbon

Organic carbon consists of primary organic carbon (POC) and secondary organic carbon (SOC). When OC/EC ratios are higher than 2.0, they indicate possible SOA (Castro et al., 1999). Since it is not possible to measure SOC directly in ambient urban air owing to the complex physical and chemical processes involved, an indirect approach was derived to estimate SOC concentrations, *i.e.* the EC-tracer method. This approach uses EC as a tracer for primary OC based on the minimum OC/EC ratio and assumes that EC is unaffected by photochemical oxidation reactions (Castro et al., 1999). Consequently, SOC and POC can be calculated using the following equations (1-3):

$$OC_{total} = POC + SOC \quad (1)$$

$$POC = EC * (OC/EC)_{min} \quad (2)$$

$$SOC = OC_{total} - POC \quad (3)$$

Where OC_{total} is the total amount of OC and $(OC/EC)_{min}$ is the minimum value of the ratio for each site during the study period (Safai et al., 2014). In this study, Organic matter (OM) was calculated as 1.4 x OC (Chow et al., 2015) to express the hydrogen, oxygen, and other elements present in organic aerosol in the ambient air.

3. Results and Discussion

3.1 Overview of PM_{10} and carbonaceous species

In general, concentrations of PM_{10}, OC and EC that are above the value of the arithmetic mean are related to meteorological variables, especially relative humidity, temperature, wind speed, wind direction and precipitation. The variation of PM_{10} mass concentrations, OC and EC with meteorological parameters at the five studied sites is shown in Figures 2. The trends presented show a high level of similarity between the different study areas, which indicates a regional characteristic to the concentrations of PM_{10}, OC and EC across NW Europe. The averages of the concentrations of PM_{10}, OC and EC for the days of sampling at the four urban background sites (AD, AP, LL and LL), and one Industrial site (WZ), are given in Table 2. Three sites presented relatively high concentrations of PM_{10} of around 30 $\mu g/m^3$, these were Antwerp (AP),

Lille (LL) and Wijk aan Zee (WZ), with average concentrations of 30.8±18.1 μg/m^3, 29.8±20.3 μg/m^3 and 29.6±16.9 μg/m^3, respectively. This initial result is in-line with a substantial body of research that has previously identified that the inner-city urban background and urban areas with industry are important sources of coarse particulate matter; here the AP and LL sampling sites were located in the centre of their respective cities, and the WZ sampling site was located in an industrial area. The Amsterdam (AD) and Leicester (LE) sampling sites were located on the outskirts of their respective city centres, with near-by arterial roads carrying typical commuter vehicular traffic. These two sites registered the lowest mean PM_{10} concentrations of the study, with averages of 25.0±15.9 μg/m^3 for AD and 20.2±14.3 μg/m^3 for LE. Being surrounded by roads, traffic is likely to be the main source of PM mass in AD and LE (Hama te al., 2017). The summary statistics for the OC and EC data over the measurement period are presented in Table 2, and Figure 2. For the measurement period, the OC and EC averages were 3.2±1.9 μg/m^3 and 0.6±0.3 μg/m^3, respectively at the urban site in Amsterdam. These concentrations were similar to those measured at the LE site, which were 3.1±1.9 μg/m^3 for OC and 0.9±0.8 μg/m^3 for EC. The OC and EC averages for the AP and LL sites were also similar, with OC values of 4.3±2.4 μg/m^3 and 4.5±2.5 μg/m^3, respectively, and EC values of 1.5±0.9 μg/m^3 and 1.2±0.6 μg/m^3, respectively. The WZ site in the industrial zone near Amsterdam city was found to have the lowest average OC and EC concentrations of 2.9±1.9 μg/m^3 and 0.7±0.7 μg/m^3, respectively. The mean OC concentrations at the four urban background sites (AD, AP, LE, LL) measured in this study ranged between 3.2 and 4.5 μg/m^3, which compares well to values reported by other investigators working in different European urban background areas (Birmingham UK, Aragéo SP, Lisbon PG) and urban/traffic zones (Ghent Belgium, Aragón Spain), as shown in Table 3. However, for the industrial site of WZ, the mean OC concentrations measured were much lower than those observed by other workers at different industrial sites in Europe and Asia, such as Pune India, Baotou China, and Delnice Croatia (Table 3). This is likely a combination of the relative amount and type of industry in the Wijk aan Zee area compared to larger industrial sites reported on in the literature, as well as the location of the industrial sources in this instance and the receptor site with respect to the prevailing wind-field. More specifically, the primary industrial sources in the area are located to the east (~750 m; energy provision) and to the south (1-2 km; steel production) of the receptor site where measurements were taken (Joaquin, 2015), whereas investigation of the meteorology data (not shown) suggests that the winds primarily originate from the west (i.e. from the coast and English Channel), with a lesser component from the south.

Similarly, for EC, measurements made here for the urban background areas of AD, AP, LE and LL were in the range reported in the literature for similar sites (Table 3). As with OC, the WZ site registered lower OC values than other industrial sites reported in the literature (Table 3).

Table 2: Overview of summary statistics (mean ± SD) of daily PM_{10} mass concentration ($\mu g/m^3$), EC, OC, OM, (total carbon) TC, POC, and SOC during the study period for the five sites.

	PM_{10}	OC	EC	TC	OC/EC	POC	SOC	OM
AD	25.0±15.9	3.2±1.9	0.6±0.3	3.8±2.1	5.7±2.8	0.7±0.3	2.5±1.8	4.5±2.7
AP	30.8±18.1	4.3±2.4	1.5±0.9	5.8±3.1	3.6±2.1	1.5±0.9	2.2±1.2	5.2±2.0
LE	20.2±14.2	3.1±1.9	0.9±0.8	4.0±2.5	4.3±2.1	1.0±0.9	2.1±1.5	4.4±2.8
LL	29.8±20.3	4.5±2.5	1.2±0.6	5.6±2.9	4.1±2.9	1.7±0.9	2.7±2.0	6.3±3.5
WZ	29.6±16.8	2.9±1.9	0.7±0.7	3.7±2.3	6.0±4.3	0.9±0.8	2.0±1.8	4.1±2.7

Table 3: Average concentrations of PM_{10}, OC and EC and OC/EC ratios in different cities across the world. Note that 'UB', 'TF', 'IN' represent urban background, traffic and industrial sites, respectively. 'NK' shows unavailability of the protocol.

Location (type of site)	N	Concentrations (µg/m3)			OC/EC	Protocol	References
		PM_{10}	EC	OC			
Amsterdam (UB)	463	25.0	0.6	3.2	5.7	NIOSH	This study
Antwerp (UB)	468	30.8	1.5	4.3	3.6	NIOSH	This study
Lille (UB)	328	29.8	1.2	4.5	4.1	NIOSH	This study

Leicester (UB)	451	20.2	0.9	3.1	4.3	NIOSH	This study
Skawina, Poland (UB)	179	80	2.4± 1.5	12.0±10.5	4.8	EUSAAR2	Błaszczak and Mathews (2020)
Bogotá, Colombia (UB)	308	37.5	3.2	8.9	3.2	EUSAAR2	Ramirez et al. (2018)
Zagreb, Croatia (UB)	121	19.4–43.6	0.6–1.6	5.0–12.0	8.5–9.2	NIOSH	Godec et al. 2016
Aragón, Spain (UB)	47	32.0	0.6	4.9	14.2	NIOSH	Escudero et al. 2015
Huelva, Spain (UB)	46	39.0	1.5	3.5	2.3	NK	Sánchez de la Campa et al. 2009
London, UK (UB)	151	23.1	2.5	5.2	2.0	NK	Harrison et al. 2004
Birmingham, UK (UB)	–	23.9	1.8	3.8	2.1	NK	Yin and Harrison 2008
Prague, Czech Republic (UB)	137	33.0	0.7	5.5	8.0	NIOSH	Schwarz et al 2008
Lisbon, Portugal (UB)	48	24.0–26.0	1.2–3.0	2.7–3.3	1.0–2.2	NIOSH	Alves et al. 2016
Mexico City, Mexico (UB)	28	74.0–95.0	4.4–5.3	14.0–17.0	3.1	NIOSH	Mugica et al. 2009
Zhengzhou, China (UB)	53	214.0	13.0	34.0	3.2	NIOSH	Wang et al. 2017
Delhi, India (UB)	24	-	2.5	10.4	5.9	IMPROVE-A	Sonwani and Saxena (2021)
São Paulo, Brazil (TF)	41	35.0	2.2	3.2	1.6	EUSAAR2	Monteiro dos Santos et al 2016
Lisbon, Portugal (TF)	48	41.0–48.0	6.0–7.4	5.5–6.8	0.9–1.0	NIOSH	Alves et al. 2016
Thessaloniki, Greece (TF)	78	42.0–51.0	1.8–2.6	7.7–8.1	2.9–4.4	NIOSH	Terzi et al. 2010
Aragón, Spain (TF)	86	25.0	1.2	4.0	4.7	NIOSH	Escudero et al. 2015
Wijk aan Zee (IN)	397	29.6	0.7	2.9	3.7	NIOSH	This study
Voivodeship of Lower Silesia, Poland (IN)	200	26.9± 13.8	0.3–13.5	2.4–26.3	2.0	EUSAAR2	Górka et al. (2020)
Pune, India (IN)	–	170.0	2.4	33.1	17.2	NIOSH	Pipal and Satsangi 2015
Delhi, India (IN)	11	174.6±64.0	58.3±46.7	79.9±44.9	3.4	IMPROVE-A	Sonwani et al (2021)
Baotou, China (IN)	402	176.0	7.7	21.8	2.8	IMPROVE	Zhou et al. 2016
Thessaloniki, Greece (IN)	81	58.0–69.0	2.9–2.9	6.4–8.7	2.2–2.9	NIOSH	Terzi et al. 2010
Bogota, Colombia (IN)	56	52.0	6.8	11.8	1.7	NIOSH	Vargas et al. 2012
Delnice, Croatia (IN)	121	19.3–47.0	0.5–2.2	5.8–18.9	10.7–14.0	NIOSH	Godec et al. 2016

279

280

281

282

283

284

285

286

287

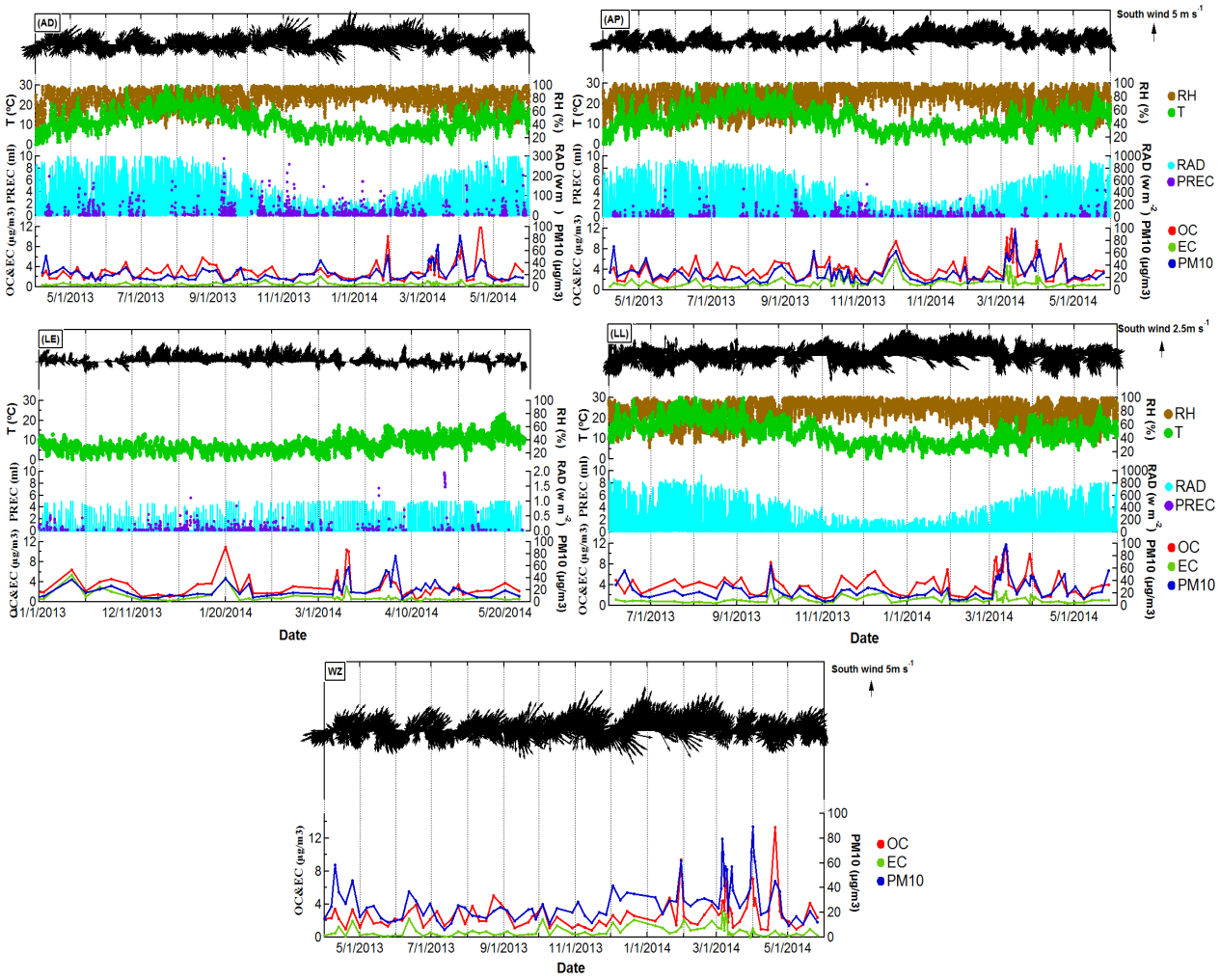

Figure 2. Temporal variation of PM_{10}, OC, EC and meteorological paramters (ws, wd, T, RH, solar radiation (RAD) and precipation) during the study period in Amsterdam, Antwerp, Leicester, Lille and Wijk aan Zee sites.

3.2 Seasonal variation of OC and EC

The monthly concentrations of EC and constituents of OC for each site during the sampling period are shown in Figures 3 and are summarized in Table S4. The results show clearly that the OC and EC concentration are higher in the cold months and lower in the warm periods. All of the sites registered the highest concentrations of OC and EC during a wave of pollution detected in the months of March and April 2014, except the LE site (we found a similar profile for PM_{10}, Figure S2). EC is a component that is related to the combustion of fossil fuels and of (diesel) traffic in particular (primary aerosol sources), while OC exists in both POA and SOA produced in complex photochemical reactions (Chen et al., 2016; Ho et al. 2002). In Amsterdam, OC showed the highest in April with a monthly mean value of 4.9 ± 4.3 µg/m^3,

while the highest EC concentration was observed during the colder months, with monthly mean values ranging from 0.7 to 0.8 μg/m^3, related to the high percentage of relative humidity. The AP and LL sites presented very similar monthly variations, with the highest concentrations of OC in Antwerp observed in March and April (at 6.8±3.2 and 7.4 ± 2.0 μg/m^3, respectively), and the highest OC concentrations measured in Lille in March (7.3±2.8 μg/m^3). At the AP site, the EC maxima was found in March and April (2.0±1.2 and 2.1±0.2 μg/m^3, respectively). For AP and LL, the lowest of EC values were observed in July. For the LE site, the highest OC averages were found in May and July (5.26±0.86 and 4.84±1.38 μg/m^3), while the highest EC levels were found in November (2.46±2.17 μg/m^3),this could be related to the high combustion of fossil fuels and upcoming traffics (diesel). At the WZ site, OC also shows a maximum concentration in April (6.99 ± 4.98 μg/m^3), while the maximum of EC were found in December, which might be related to the high biomass combustion sources in the area. It can be noted that all sites showed higher OC concentrations during spring (March-May). This can be associated with a combination of meteorological conditions and various emission sources that led to highly elevated OC concentrations in this region in spring, mainly due to high temperatures which cause increased photochemical reactions. This result indicates the influence of additional sources of carbonaceous aerosols, e.g. SOC formation (Section 3.5) can also influence OC concentrations. The highest OC concentrations may also be related to other sources of PM_{10}, such as mineral dust transport and inorganic aerosol, which were predominant in spring (Hama et al., 2018). Moreover, the high contributions during spring could also be attributed to agricultural activities (Joaquin, 2015). The bonfire activities during Easter are also responsible for some of the high contributions during this period. The contribution of bonfires is primarily driven by the presence of OC (markers for biomass burning).

For EC, the highest concentrations were found during colder months (November and December), except Antwerp. This can be mainly associated with increased coal consumption related activities and unfavourable dispersion conditions in winter season. Moreover, previous studies highlighted that EC concentrations vary seasonally, with higher concentrations being recorded during the colder months, indicating that emissions from fossil fuel combustion for residential heating are a significant source of EC in particulate matter in winter (Błaszczak and Mathews, 2020; Cesari et al., 2018; Górka et al., 2020; Sonwani and Saxena, 2021; Sonwani et al., 2021). For example, elemental carbon showed higher winter concentrations at an urban background site in Italy, in agreement with the major local primary emission sources from combustion processes (i.e. domestic heating and biomass burning) (Cesari et al., 2018). Higher

EC concentrations in particulate matter usually indicate a major contribution from the combustion of liquid fossil fuels, especially from road traffic (Cesari et al., 2018; Górka et al., 2020). In addition, differences in meteorological conditions in the measuring location may also be possibly attributed to the discrepancy in OC and EC concentrations in PM_{10}. In general, an increase in carbonaceous species of local/regional origin can be seen, particularly under low wind speed and poor pollutant dispersion (Górka et al., 2020). We can thus conclude that carbonaceous aerosols show that the location of the monitoring station relative to the emission sources is one of the most crucial factors controlling OC and EC concentrations in PM_{10}. The OC/EC ratio can be used to investigate the impact of aerosols on climate forcing (Novakov et al., 2005; Mbengue, et al., 2018). This species has been extensively identified in both biomass/biofuel and fossil fuel combustion sources, and many studies recommend OC/EC correlation to improve the sources and aerosol light absorption analysis (Lu et al., 2015). The EC/OC at the AP, LE and LL sites showed relatively low correlation (R^2=0.42, 0,44 and 0,41 respectively, Figure 4). This is clearly indicated that the EC and OC concentration are influenced by different emission sources at those three sites. In addition, the OC/EC ratio at the AD and the industrial (WZ) sites showed relatively very lower correlation (R^2=0.11 and 0,18 respectively). This can also indicated that the OC and EC affected by very different emission sources at both sites, which might be related to the industrial source. Probably the poor correlation is because OC contains SOC. In addition, the correlation between OC and EC varied by season (Hama et al., 2018) and was highest in the cold (heating) season, reflecting the contribution of biogenic, non-EC sources, while the lowest in the vegetative season due to primary biological aerosol particles (Yttri, et al., 2021). In addition, in order to explain the OC and EC weak corelations, we plot the correlation between SOC vs OC and OC vs EC are shown in Figures S3 and S4. The highest correlation found between SOC vs OC in all cities, indicating that the poor correlation between OC and EC owing to OC contains SOC. Similar correlation was found between POC and EC, indicating the EC is influenced by the primary aerosol particles in studied sites.

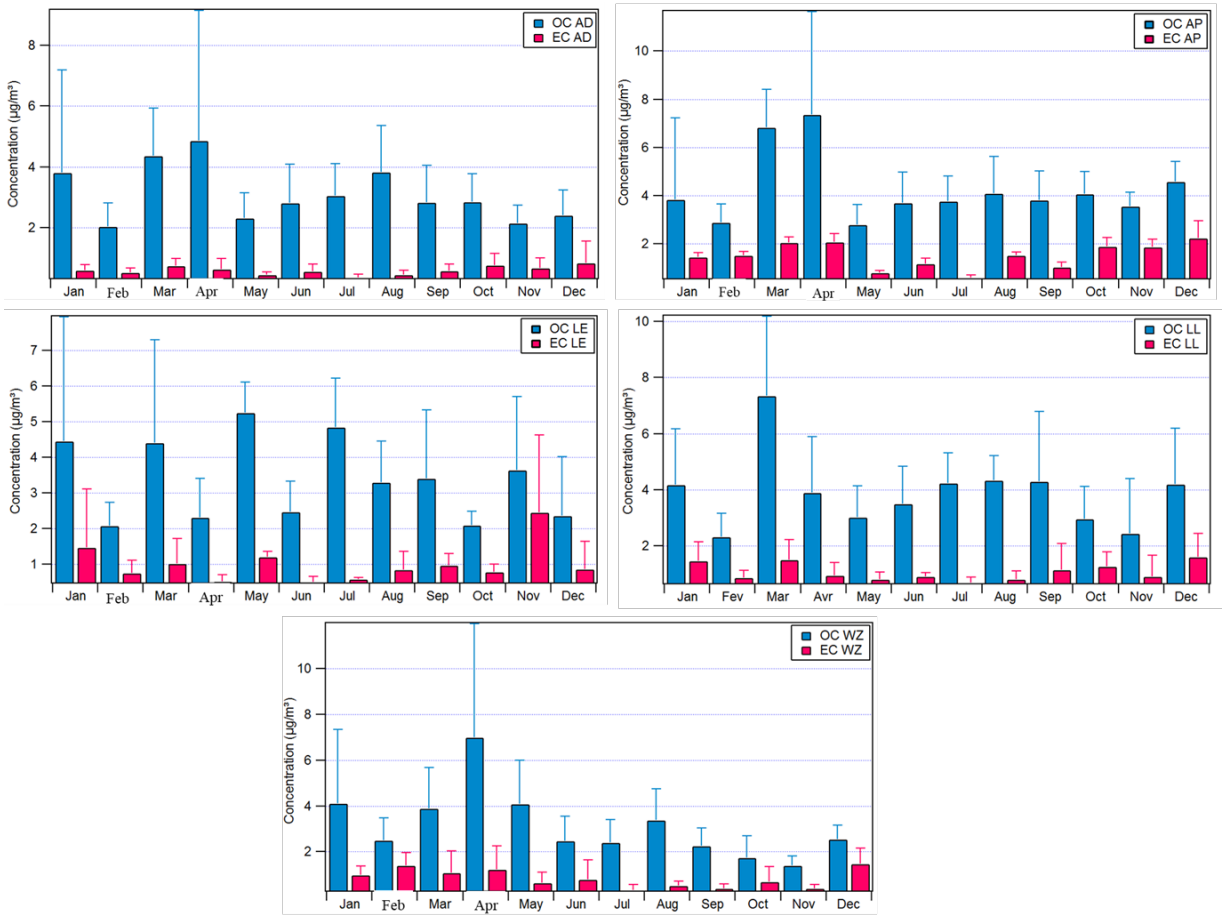

380

381

382 **Figure 3.** Monthly variation of OC and EC during the study period in Amsterdam, Antwerp,

383 Leicester, Lille and Wijk aan Zee sites.

384

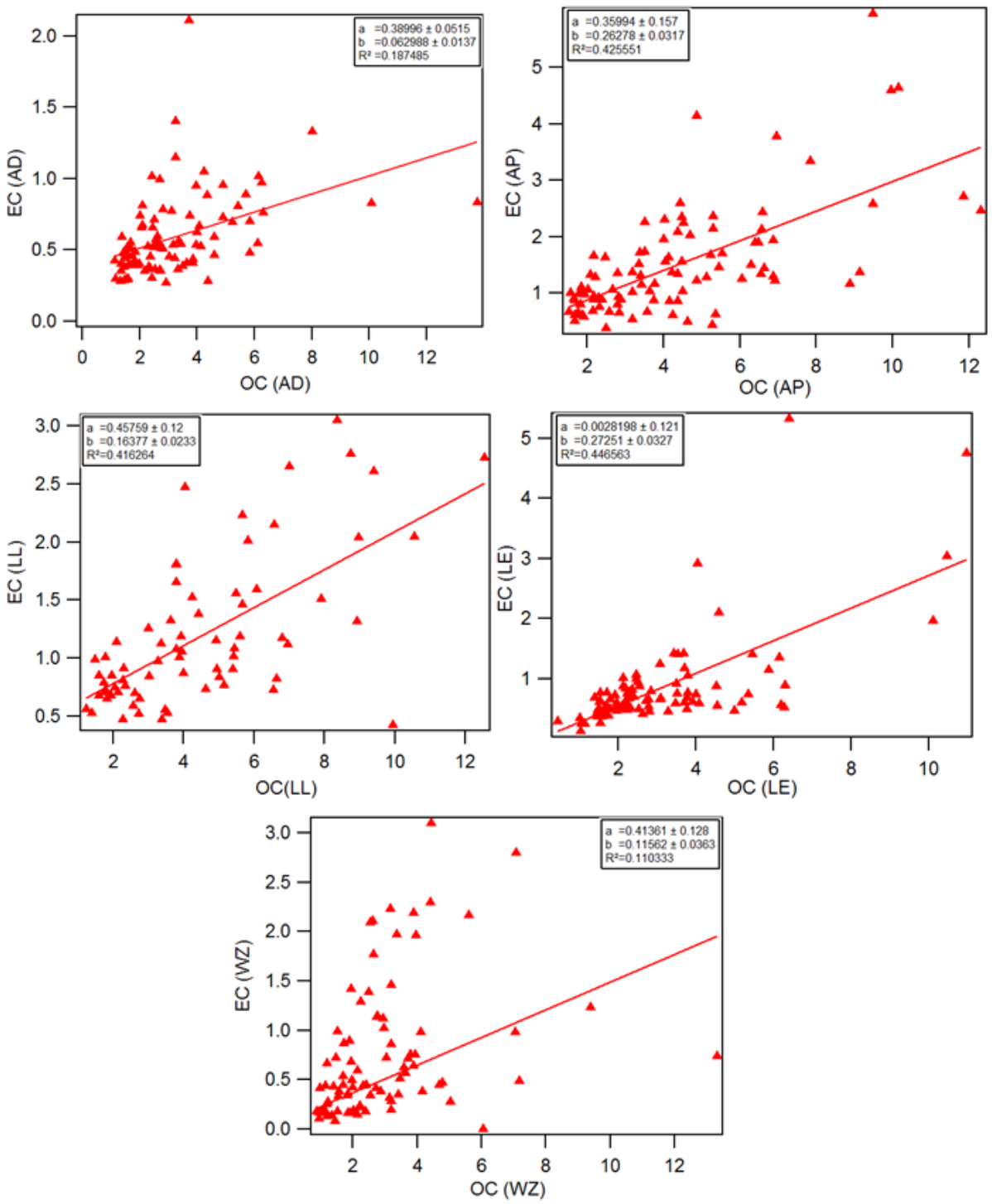

385

386 **Figure 4.** Correlation between EC and OC for the five sites during the study period.

387

388

389

390

391

3.3 Contribution of carbonaceous aerosol to PM_{10}

The average contributions of TC (OC and EC) to the total measured PM_{10} mass were 15.2% 18.8%, 19.8%, 18.8% and 12.5%, for AD, AP, LE, LL and WZ, respectively. These values are consistent with results obtained from other European sites (Cavalli, et al., 2016; Lonati et al., 2007, Sánchez de la Campa et al., 2009), where it was found that TC accounted for between 10% and 50% of total PM_{10}. The result obtained here was slightly lower than that of urban areas in Zhengzhou (22%, Wang et al., 2017) and Ghent (22%, Viana et al., 2006). In terms of the carbonaceous fractions, OC accounted for 12.8%, 13.9%, 15.3%, 15.1% and 9.8%, and EC accounted for 2.4%, 4.9%, 4.4%, 4.0%, and 2.4% of total PM_{10} mass for AD, AP, LE, LL and WZ, respectively (Table 3). Interestingly, the highest percentage of OC was found in LE (EC at the AP), while the lowest was in WZ (EC at the AD). This may have been an impact of the location of the sampling sites (Table 1), where AP and LE had higher traffic intensity, and hence higher traffic related emissions, than the other sites which leads to increased OC and EC levels. At the AD site, the highest contribution of TC to PM_{10} was found in October (24.1%), whilst the lowest contribution was found in March (11.6%, Table S4). At the AP and LE sites, the highest contributions of TC to PM_{10} were observed in October (25.2%) and August (31.8%), whilst the lowest contributions were found in May (10.8%) and April (10.5%, Table S4) respectively. In the LL and WZ sites, the highest contributions of TC to PM_{10} were found in December (27.5%) and August (20.6%), whilst the lowest contributions were found in May (13.7%) and November (9.4%, Table S4) respectively. Interestingly, TC shows the highest percentage in August at the WZ site. This may be associated with primary biological organic aerosol and SOA which showed high contributions to PM_{10} in north-west Europe (Glasius et al., 2018). In addition, previous studies all report the same key findings; OC from residential wood burning emissions (domestic) dominate during the cold (heating) period and SOA originating from biogenic sources is the most important fraction of the carbonaceous aerosol in summer across north-Europe (Glasius et al., 2018; Noziere et al., 2015). From this it can be seen that the average mass concentrations of EC, OC and TC at all sites were relatively higher during colder months than during warmer parts of the year (Table S4). This may be a result of biomass activities during colder periods, which is consistent with previous (Cordell et al., 2016), which found the levels of the biomass burning marker, levoglucosan, to be higher during the colder months. It was also found that the average value of OM accounted for 20.2%, 21.7%, 26.2%, 23.2%, 15.1% of PM_{10} mass concentration for the AD, AP, LE, LL and WZ, respectively (Table S4). This is consistent with earlier studies reporting OM in London (~21%,

Harrison et al., 2004); Hong Kong (~20%, Ho et al., 2003) and Thessaloniki (22%, Terzi et al., 2010). However, the results were slightly lower than those reported in Bogota (42%, Ramírez et al., 2018); Barcelona (33%, Viana et al., 2007); Dar es Salaam (37%, Mkoma et al., 2009); Elche (40%, Galindo et al., 2020); Zurich (52%, Lanz et al., 2010); and Prague (45%, Kubelová et al., 2015). The contribution of OM increased during summer at four sites, which accounted for 24.9%, 25.4%, 31.5%, and 19.9% in AD, AP, LE and WZ sites, respectively. Higher OM in summer is most likely a result of photochemical oxidation of both anthropogenic and biogenic precursors leading to SOA formation (Hallquist, et al., 2009). Conversely, the highest OM levels in LL were observed in winter, at 28%, and the lowest in spring, at 17.2% (Table S4). Higher OM during winter at the LL site may have resulted from periods of limited dispersion conditions and the decrease in ambient temperatures that leads to higher condensation of semi-volatile organic compounds (Galindo et al., 2019). It is well known that meteorological conditions have an impact on the formation of OC from gas-to-particle conversion processes and the concentration of POA and fresh SOC (which changes the OM/OC ratio), as does regional and long-range transport of organic aerosols at different times of the year (Aiken et al., 2008),

3.4 The OC/EC ratio

OC/EC ratios are a valuable tool to indicate the sources and processes of carbonaceous particle matter formation. At the AD and WZ sites, the OC/EC ratio ranged from 3.6 (November) to 9.2 (July) and from 1.8 (February) to 16.2 (May) (Table 2 and 3), with annual average values of 5.7±2.8 and 6.0±4.3, respectively. For LL and AP, the two sites measuring the highest values of OC, the ratio OC/EC ranged from 2.4 (October) to 6.1 (July) and from 1.9 (February) to 7.0 (July), with annual average values of 4.1±2.9 and 3.6±2.1, respectively. For LE the OC/EC ratio ranged from 2.0 (November) to 9.1 (May), with an annual average value of 4.3±2.1. These findings are in line with other, similar studies carried out in in Ghent, Belgium (3.5, Viana et al. 2006), but slightly lower that findings reported in Zagreb, Croatia (8.5-9.2, Godec et al. 2016) and Aragon Spain (14.2, Escudero et al. 2015). In general, high OC/EC ratios are consistently associated with low EC concentrations and low ratios with high EC values (Novakov et al., 2005). Atmospheric conditions, temperature inversions, emission sources, and SOC contributions are the principal determining factors to the variations of the value of OC/EC. However, the results for Amsterdam and Lille in this study indicate a slightly different pattern, in which OC/EC ratios appear mainly related to variations of OC

concentrations. All sites examined here were found to have mean OC/EC values >2, which indicates the existence of SOC (Cong et al. 2015; Liu et al. 2016). Looking at the monthly averages, it appears that the carbonaceous fraction measured at all sites was dominated by secondary sources, with the exceptions of Wijk aan zee and Antwerp, which appear to have been influenced by primary sources in February, where the ratio OC/EC ratio ranged between 1.5 and 2. With the exception of July and August, the high OC/EC ratios registered in this study strongly suggest that during the sampling year there were significant levels of SOC. It is also possible that there were contributions to SOC from aged aerosols following long-distance transport (Mancilla et al., 2015).

3.5 Variability of SOC concentrations

The estimation of SOC is vital as it plays a significant role in the formation of haze (and hence visibility degradation), climate and health. Absolute values of POC and SOC are important when attempting to understand atmospheric aging processes of organic aerosols in urban areas, and ultimately in the design of effective emission control policies. In order to estimate contributions of POA and SOA to the total PM_{10} mass concentration, the EC-tracer method has been widely used in many studies (Galindo et al., 2019; Kim et al., 2020; Liao et al., 2020; Shivani et al., 2020; Xie et al., 2020), and is employed here (as described in Section 2.3). To gain insights into factors controlling the formation of SOA, monthly concentrations of POC and SOC were determined for the five sites and are shown in Figures 5. Average SOC (POC) concentrations measured here were 2.5±1.8 (0.7±0.3), 2.2±1.2 (1.5±0.9), 2.1±1.5 (1.0±0.9), 2.7±2.0 (1.7±0.9), and 2.0±1.8 (0.9±0.8) $\mu g/m^3$, for AD, AP, LE, LL and WZ sites, respectively (Table 2). In addition, at the AD, AP and WZ sites, SOC showed the highest in April, followed by March-May and July-August January for the WZ site), while the SOC showed the lowest during November- December, February (Figure 6, Table S4). At LE site, SOC showed the highest in July, followed by May and March, while the SOC showed the lowest in November (Figure 8, Table S4). At LL site, SOC showed the highest in March, followed by July and August, while the SOC showed the lowest in February (Figure 5, Table S4). The significant contribution of SOC in the spring/summer corresponds to high potential photochemistry and low contributions of POC from local primary emission sources, most likely from traffic and coal combustion (Mbengu et al., 2018;). Previous study revealed that SOC displays a similar pattern to3 ozone at noon, following the maximum photochemical activity and solar radiation intensity (Mbengu et al., 2018). The above results show that SOC particles observed in this

study were a significant component of the OC mass in all five sites. In particular, the higher percentage of SOC in spring/summer, observed at the five sites, can be attributed to several factors. In spring/summer, a higher contribution of OC may be anticipated considering the increased emission of VOCs from the vegetation and the enhanced photochemical activity supporting SOA formation which leads to increased SOC (Bencardino, et al., 2019). In general, for the five measurement sites investigated here, SOC concentrations showed a roughly seasonal cycle characterised by maxima occurring during spring and summer and minima occurring during late autumn and winter (Figure 5, Table S4). This result is consistent with SOC formation coinciding with periods of the year that had relatively higher temperatures and more solar radiation, and hence photochemical activity (Bencardino, et al., 2019; Dinoi et al., 2017), including ozone chemistry (Kim et al., 2012). The results obtained here are in-line with those reported in other studies (Pio et al., 2011; Safai et al., 2014), but in disagree with others in China (Ji et al., 2016; Wang et al., 2017), India (Shivani et al., 2019) and some European cities (Godec et al., 2016; Galindo et al., 2019), where high SOC concentrations were noted in winter In this study, photochemical activity and atmospheric temperature appear to play important roles in SOC formation at the five study sites. Interestingly, SOC levels were relatively higher in January (winter season at all sites) at the AD, AP, LE and WZ sites (Figure 5, Table S5). It is likely that this was primarily a result of lower temperatures accelerating the condensation of volatile organic compounds onto particulate matter (Galindo et al., 2019). The prevailing meteorology during these episodes is favourable for the formation and build-up of secondary organic pollutants. The prolonged residence time of stable atmospheric conditions strengthens atmospheric oxidation and low temperature (and high relative humidity) which would enhance the condensation of volatile secondary organic compounds on pre-existing aerosols. Seasonal contribution of POC and SOC to OC is presented in Figures 6. It was observed that SOC contributed more than POC to total OC during spring and summer months at the five sites. More specifically, SOC contributed ~ 77%, 50%, 67%, 60% and 69% to OC and 10%, 7%, 10%, 9% and7% to PM_{10} at the AD, AP, LE, LL and WZ sites, respectively, during the study period. The SOC contributions to OC found in this study, were higher than those reported by Ramírez et al. (2018) in Bogota, and by Shivani et al. (2020) in Delhi, who found lower percentages of ~44% and ~46% for the SOC contribution to OC. In summary, at the five study sites investigated in this study, SOC contributions appeared to be greater during relatively warmer months compared to colder months, each of the five sites showed similar patterns of SOC concentrations and SOC contributed more than POC in each case.

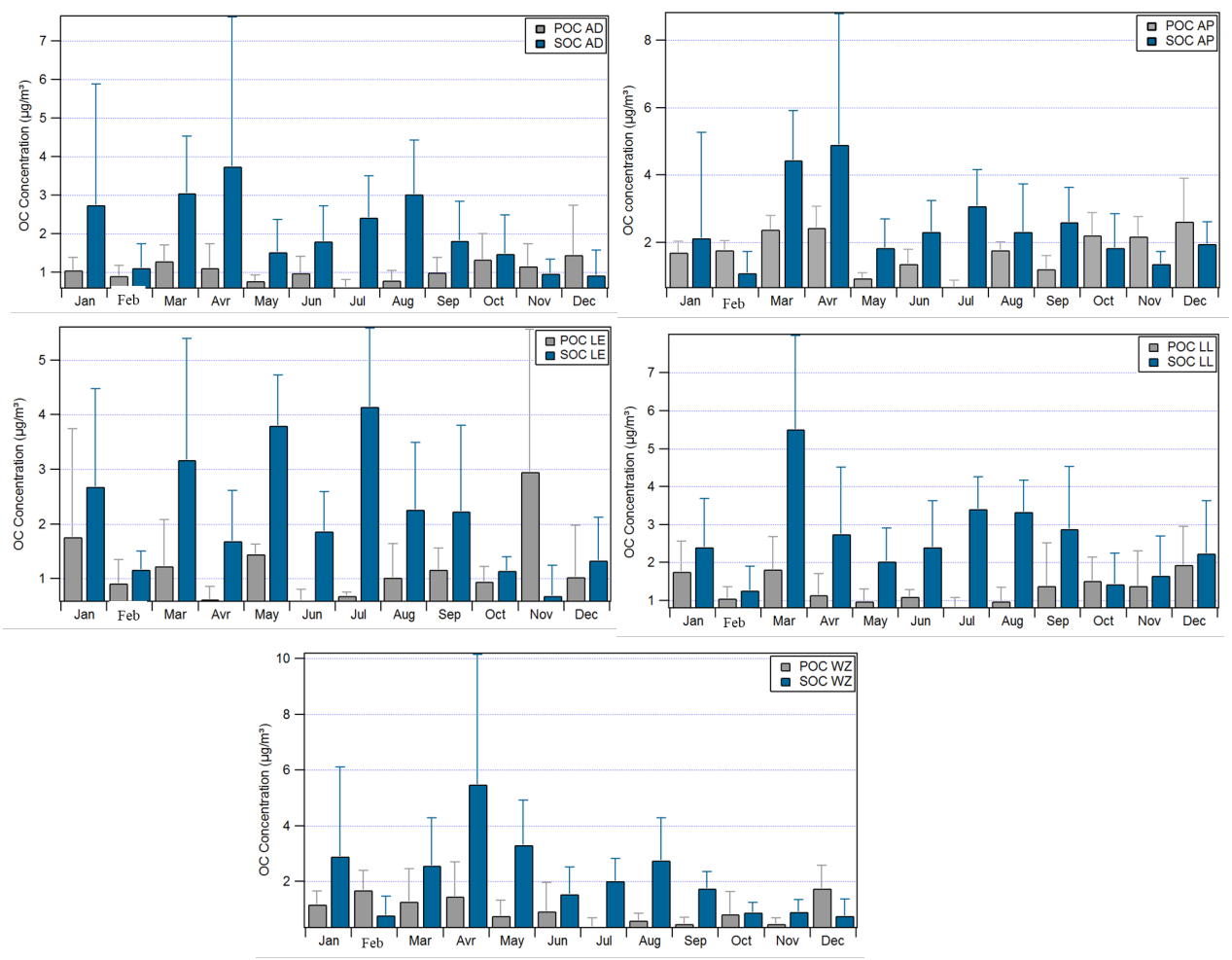

Figure 5. Monthly variation of SOC and POC during the study period in Amsterdam, Antwerp, Leicester, Lille and Wijk aan Zee sites.

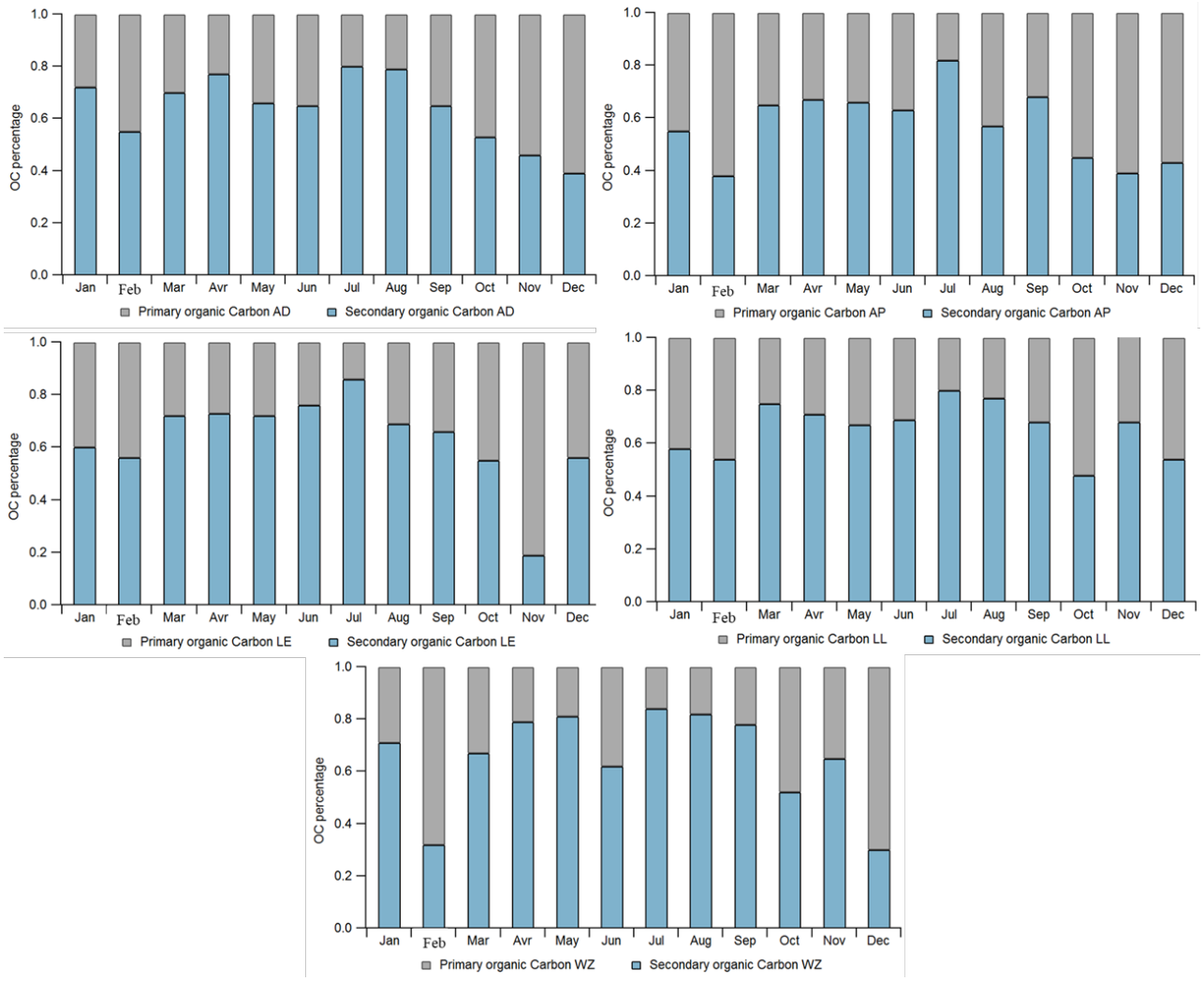

Figure 6. Monthly contribution (%) of SOC and POC during the study period in AM, AP, LE, LL and WZ sites.

3.6 Effective carbon ratio

Atmospheric particles have a significant role in determining the Earth's energy balance, directly by scattering and/or absorbing solar radiation and indirectly by serving as cloud condensation and ice nuclei for cloud droplet activation, which alters the radiative and microphysical properties, and lifetime of clouds (Stocker et al., 2013; IPCC, 2014; Wang et al., 2013; Wu et al., 2020). Scattering and absorption characteristics are two vital parameters in determining the effect of atmospheric particles on the Earth's radiative balance. The radiative forcing of atmospheric particles can exert both positive and negative forcing. For instance; POC plays a significant role in direct radiative forcing as a potential light-absorbing species (IPCC, 2014), and hence it contributes to global warming (Bond et al., 2013). However, SOC generally originates from the oxidation of various types of volatile organic compounds (VOCs) and scatters solar radiation (Pandis et al., 1992). Recently, Safai et al. (2014) proposed the concept of ECR to obtain a better association between atmospheric carbonaceous aerosols and climate change. This approach has been widely used in previous studies (Safai et al., 2014; Singh et al., 2015; Pipal and Satsangi, 2015; Ramírez et al., 2018; Pani et al., 2019). Figure 7 shows the monthly ECR values, which were calculated using equation 4 (Safai et al., 2014).

$$ECR = SOC / (POC+EC) \quad (4)$$

According to Safai et al. (2014), a higher ECR value indicates low POC and EC, which could suggest higher levels of direct radiative forcing. This also could lead to a reduction in atmospheric warming effect of combustion aerosols and increase the scattering properties of radiation. In this study, ECR values ranged between 0.7±0.4 (November) and 2.7±1.5 (July); 0.3±0.2 (February) and 2.7 ± 1.7 (July); 0.4±0.3 (November) and 3.3 ± 1.3 (July); 0.5±0.3 (October) and 2.2 ± 0.1 (July); and 0.3±0.2 (February) and 6.2 ± 3.5 (May) (Figure 8) for the AD, AP, LE, LL, and WZ sites, respectively. Interestingly, the highest ECR values were observed in April and May at the WZ site. This indicates the predominance of scattering carbonaceous aerosols and a reduction in atmospheric warming. This can also be related to higher SOC in spring (Section 3.5), indicating the larger formation of SOC in the spring season. And also the occurrence of in-cloud SOA formation and the role of heterogeneous chemistry might also be attributed at the WZ site. This result is consistent with the findings of Section 3.5 which showed that the highest SOC in April and May at the WZ site. In general, ECR values >2.0 were obtained in April, May and July (Figure 7), during which time higher concentrations of SOC than POC were observed (Figure 5). Lower ECR values (≤0.3) in

October, November and February at all the sites were mostly due to the higher concentrations of total POC and EC and lesser contribution from SOC, indicating greater proportional formation of SOC has greater propensity to scatter solar radiation. However, higher values of ECR in April, May and July have implications for more absorbing types of carbonaceous aerosols. These findings are consistent with previous studies (Pipal and Satsangi, 2015; Pani et al., 2019), which also found high levels of ECR in July. In addition, the ECR annual mean values were 1.4, 1.0, 1.5, 1.2 and 2.5 for the sites in AD, AP, LE, LL, and WZ, respectively. The annual mean determined here was relatively higher (1.0-2.5) than earlier studies reporting (0.5-0.55) in urban areas (Safai et al., 2014; Ramírez et al., 2018; Pani et al., 2019).

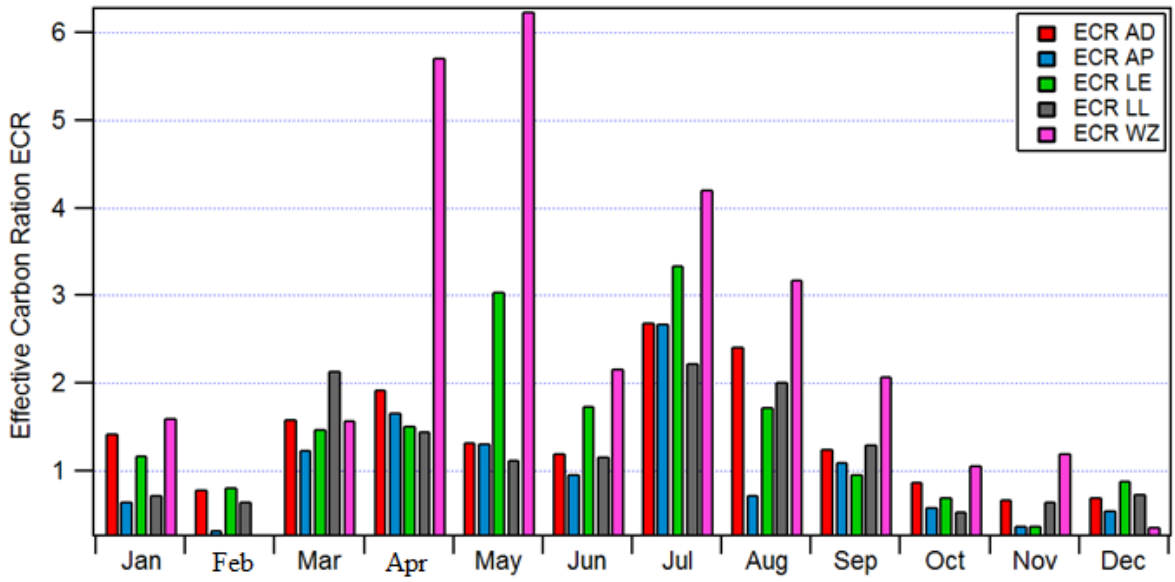

Figure 7. Monthly variation of effective carbon ratio at the five measurement sites during study period.

3.7 Air masses backward trajectories

In order to investigate the potential origin of particles investigated in this work, air mass back trajectories were determined using the NOAA HYSPLIT model. When deconvoluting particle composition it is important to consider chemical transformation and aging, e.g. the SOC fraction collected and reported here could have had its origins only locally, but it could also have been incorporated into the particle during air mass transport, after which it would have been subject to potential chemical transformation as the air mass moved from one regional to another (Schwarz et al., 2008; Sánchez De La Campa et al., 2009; Peng et al., 2016). Cluster analysis can be used to describe the characteristics of trajectories having different origins and pathways and helps to explain the variability of trajectories associated with different processes

(Pérez et al., 2015). In this study the clusters of backward trajectories were calculated during warm and cold periods (March-May and December-February 2014) at 300m height (Stein et al., 2015) for each of the five studied sites (Figures 8 and S5-9). The clustering results are sensitive to the meteorological data output from the Global Data Assimilation System (GDAS) running with the HYSPLIT model. According to the results of the back-trajectory simulations, 90% of the air masses were from continental origin for both LL and AP sites between March, April and May 2014 (Figures 8 and S5-9), originating from the southern and northern UK, and transported over long distances. During the cold period, more than 95% of the air masses coming from west, and south west, the majority of the air masses were from continental origin for all the studied sites which explain the decrease of the temperature during those months (Figures S5-9). This means that the contributions of Carbonaceous aerosols coming from the continental origin and the other cities could be detected during this period in the studied sites. The high OC concentrations detected during this period were most probably related to strong local emissions of OC and SOC precursor gases capable of spreading over large areas, and being transported over long distances (Pandolfi, et al., 2020; Vicente et al., 2018). We observe the same behaviour for the other three sites (LE-AD-WZ), the highest concentration of OC and SOC detected in the most polluted period (between Mach and April 2014), was most probably related to air masses arriving at the sampling sites from local or well as regional areas. The fast-flowing air mass accounts for more than 90% of the trajectories and was predominantly coming from the north and northeast.

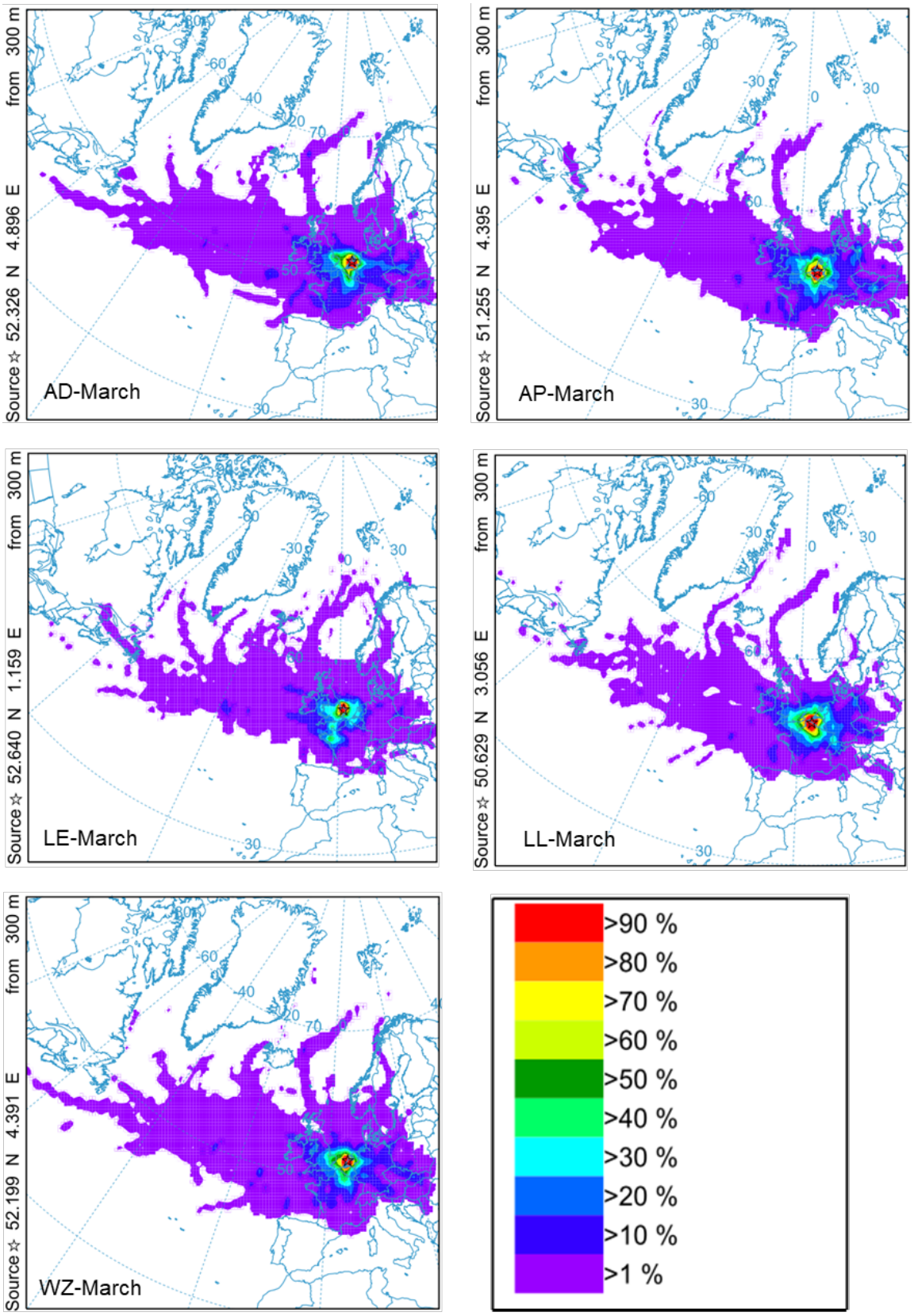

Figure 8. The backward trajectory frequency for the five studied sites at 300m AGL, for March 2014, calculated by the HYSPLIT Model.

4. Conclusions

To understand the characteristics of PM_{10}-associated OC and EC, and to investigate the Spatial and seasonal variations of the carbonaceous aerosols at four urban background sites located in Amsterdam (AD), Antwerp (AP), Leicester (LE) and Lille (LL), and one industrial site at Wijk aan Zee (WZ) across North-West Europe, ~2,000 PM_{10} samples were simultaneously collected. The highest OC concentrations were found in March-May in most cities, which indicates a combination of meteorological conditions and various emission sources that led to highly elevated OC concentrations in this region. However, the highest EC concentrations were found during colder months (November and December), except Antwerp. This can be mainly associated with increased coal consumption during the heating season and unfavourable dispersion conditions. Probably the poor correlation between OC and EC might be because OC contains SOC. The average contributions of total carbon (OC and EC) to the total measured PM_{10} mass were 15.2% 18.8%, 19.8%, 18.8% and 12.5%, for AD, AP, LE, LL and WZ, respectively. It can be seen that the average mass concentrations of total carbon and TC at all sites were relatively higher during colder months than during warmer months which indicates increasing biomass activities in winter season. Notably, TC shows the highest percentage in August at the WZ site, indicating primary biological organic aerosol and SOA which showed high contributions to PM_{10} across north-west Europe. SOC contributed ~ 77%, 50%, 67%, 60% and 69% to organic carbon and 10%, 7%, 10%, 9% and7% to PM_{10} at the AD, AP, LE, LL and WZ sites, respectively. The significant contribution of SOC in the spring/summer links to high potential photochemistry and low contributions of POC from local primary emission sources. ECR values >2.0 were obtained in spring and summer, during which time higher concentrations of SOC than POC were observed. However, lower ECR values ($\leq$0.3) in winter season at all the sites were mostly due to the higher concentrations of total POC and EC and lesser contribution from SOC, indicating greater proportional formation of SOC has greater propensity to scatter solar radiation. Higher values of ECR in spring/summer have implications for more absorbing types of carbonaceous aerosols. Monthly air mass backward trajectory cluster was calculated during warm and cold periods at 300m height for the five sites. The back-trajectory simulations showed that 90% of the air masses were from continental origin for both LL and AP sites between March, April and May 2014, originating from the southern and northern UK, and transported over long distances. During the cold period, more than 95% of the air masses coming from west, and south west, the majority of the air masses were from continental origin for all the studied sites which explain the decrease of the temperature during

those months. This study examined a comprehensive one-year intensive measurement campaign, where organic carbon (OC) and elemental carbon (EC) fractions of PM_{10} were measured in the North-West European 'air pollution hotspot' region. Owing to the importance of carbonaceous aerosols in understanding particulate pollution sources and its impact on human health and environment, the hourly online OC and EC measurements are worth investigating in the future. Measurements of VOCs and polycyclic aromatic hydrocarbon (PAHs) were not made in this study due to practical constraints, such as the availability of similar sets of instruments across the region. Thus, further studies are recommended to investigate the concentrations of VOCs and PAHs simultaneously for a more holistic investigation across North-West Europe.

5. Acknowledgements

This research was funded by the Joint Air Quality Initiative (JOAQUIN) project, part of the EU Interreg IV-B NWE Program. We thank the NOAA ARL for computing air mass back trajectories using the HYSPLIT model. We also thank reviewers for contributions to improve the quality of the paper.

6. CRediT authorship contribution statement

Sarkawt Hama: Writing-Original Draft, Investigation, Formal analysis, Data curation, Resources, Conceptualization, Methodology, Visualization, Validation, Writing - review & editing. **Ibrahim Ouchen:** Formal analysis, Writing - Original Draft, Writing - review & editing. **Kevin Wyche**: Writing - Original Draft, Writing - review & editing. **Rebecca Cordell:** Investigation, Data curation, Resources, Writing - review & editing. **Paul Monks:** Conceptualization, Funding acquisition, Supervision, Writing - Original Draft, Writing - review & editing.

7. Declaration of interest

The authors declare no conflict of interest.

6. References

Alves, A., Oliveira, C., Martins, N., Mirante, F., Caseiro, A., Pio, C., Matos, M., Silva, H., Oliveira, C., Camões, F., 2016. Road tunnel, roadside, and urban background measurements of aliphatic compounds in size–segregated particulate matter. Atmos. Res.168, 139–148.

Aiken, A.C., Decarlo, P.F., Kroll, J.H., Worsnop, D.R., Huffman, J.A., Docherty, K.S., Ulbrich, I.M., Mohr, C., Kimmel, J.R., Sueper, D. and Sun, Y., 2008. O/C and OM/OC ratios

of primary, secondary, and ambient organic aerosols with high-resolution time-of-flight aerosol mass spectrometry. Environmental science & technology, 42, 4478-4485.

Bencardino, M., Andreoli, V., D'Amore, F., Simone, F.D., Mannarino, V., Castagna, J., Moretti, S., Naccarato, A., Sprovieri, F. and Pirrone, N., 2019. Carbonaceous aerosols collected at the observatory of Monte Curcio in the Southern Mediterranean Basin. Atmosphere, 10, 592.

Biswas, S., Verma, V., Schauer, J.J., Cassee, F.R., Cho, A.K. and Sioutas, C., 2009. Oxidative potential of semi-volatile and non-volatile particulate matter (PM) from heavy-duty vehicles retrofitted with emission control technologies. Environmental Science & Technology, 43, 3905-3912.

Błaszczak, B. and Mathews, B., 2020. Characteristics of carbonaceous matter in aerosol from selected urban and rural areas of Southern Poland. Atmosphere, 11, 687.

Bond, T.C., Doherty, S.J., Fahey, D.W., Forster, P.M., Berntsen, T., DeAngelo, B.J., Flanner, M.G., Ghan, S., Kärcher, B., Koch, D. and Kinne, S., 2013. Bounding the role of black carbon in the climate system: A scientific assessment. Journal of geophysical research: Atmospheres, 118, 5380-5552.

Castro, L.M., Pio, C.A., Harrison, R.M. and Smith, D.J.T., 1999. Carbonaceous aerosol in urban and rural European atmospheres: estimation of secondary organic carbon concentrations. Atmospheric Environment, 33, 2771-2781.

Cavalli, F., Alastuey, A., Areskoug, H., Ceburnis, D., Čech, J., Genberg, J., Harrison, R.M., Jaffrezo, J.L., Kiss, G., Laj, P. and Mihalopoulos, N., 2016. A European aerosol phenomenology-4: Harmonized concentrations of carbonaceous aerosol at 10 regional background sites across Europe. Atmospheric Environment, 144, 133-145.

Cesari, D., Merico, E., Dinoi, A., Marinoni, A., Bonasoni, P. and Contini, D., 2018. Seasonal variability of carbonaceous aerosols in an urban background area in Southern Italy. Atmospheric Research, 200, 97-108.

Chen, Y., Shen, G., Huang, Y., Zhang, Y., Han, Y., Wang, R., Shen, H., et al., 2016. Household air pollution and personal exposure risk of polycyclic aromatic hydrocarbons among rural residents in Shanxi, China. Indoor Air 26, 246–258.

Chow, J.C., Lowenthal, D.H., Chen, L.W.A., Wang, X. and Watson, J.G., 2015. Mass reconstruction methods for $PM_{2.5}$: a review. Aai Qual. Atmos. Hlth., 8, 243-263.

CoA, 2020. City of Amsterdam Low Emission Zone online. Available online at: https://www.amsterdam.nl/en/traffic-transport/low-emission-zone/. (accessed 21 February 2021).

Cong Z., Kang S., Kawamura K., Liu B., Wan X., Wang Z., Gao S., Fu P., 2015. Carbonaceous aerosols on the south edge of the Tibetan plateau: concentrations, seasonality and sources. Atmos Chem Phys 15:1573 – 1584.

Cordell, R.L., Mazet, M., Dechoux, C., Hama, S.M.L., Staelens, J., Hofman, J., Stroobants, C., Roekens, E., Kos, G.P.A., Weijers, E.P. and Frumau, K.F.A., 2016. Evaluation of biomass burning across North West Europe and its impact on air quality. Atmospheric Environment, 141, 276-286.

DfT, 2020, Department for Transport 2020. Map Road Traffic Statistics - Road Traffic Statistics. Online Available at: https://roadtraffic.dft.gov.uk/manualcountpoints/ . (accessed 21 February 2021).

De Gouw, J. and Jimenez, J.L., 2009. Organic aerosols in the Earth's atmosphere.

EEA, 2019. Air Quality in Europe European Environment Agency, Luxemburg (2019). https://www.eea.europa.eu/publications/air-quality-in-europe-2019 (accessed 21 February 2021).

Didyk, B., Simoneit, B., Pezoa, L., Riveros, M., Flores, A., 2000. Urban aerosol particles of Santiago, Chile: organic content and molecular characterization. Atmos. Environ. 34, 1167–1179.

Dinoi, A., Cesari, D., Marinoni, A., Bonasoni, P., Riccio, A., Chianese, E., Tirimberio, G., Naccarato, A., Sprovieri, F., Andreoli, V. and Moretti, S., 2017. Inter-comparison of carbon content in $PM_{2.5}$ and PM_{10} collected at five measurement sites in Southern Italy. Atmosphere, 8, 243.

Escudero, M., Viana, M., Querol, X., Alastuey, A., Díez Hernández, P., García Dos Santos, S., Anzano, J., 2015. Industrial sources of primary and secondary organic aerosols in two urban environments in Spain. Environ. Sci. Pollut. Res. 22, 10413–10424.

Fan, J., Rosenfeld, D., Ding, Y., Leung, L.R. and Li, Z., 2012. Potential aerosol indirect effects on atmospheric circulation and radiative forcing through deep convection. Geophysical Research Letters, 39, L09806.

Fuzzi, S., Andreae, M.O., Huebert, B.J., Kulmala, M., Bond, T.C., Boy, M., Doherty, S.J., Guenther, A., Kanakidou, M., Kawamura, K. and Kerminen, V.M., 2006. Critical assessment of the current state of scientific knowledge, terminology, and research needs concerning the role of organic aerosols in the atmosphere, climate, and global change. Atmospheric Chemistry and Physics, 6, 2017-2038.

Galindo, N., Yubero, E., Clemente, A., Nicolás, J.F., Navarro-Selma, B. and Crespo, J., 2019. Insights into the origin and evolution of carbonaceous aerosols in a mediterranean urban environment. Chemosphere, 235, 636-642.

Galindo, N., Yubero, E., Clemente, Á., Nicolás, J.F., Varea, M. and Crespo, J., 2020. PM events and changes in the chemical composition of urban aerosols: A case study in the western Mediterranean. Chemosphere, 244, 125520.

Glasius, M., Hansen, A.M.K., Claeys, M., Henzing, J.S., Jedynska, A.D., Kasper-Giebl, A., Kistler, M., Kristensen, K., Martinsson, J., Maenhaut, W. and Nøjgaard, J.K., 2018. Composition and sources of carbonaceous aerosols in Northern Europe during winter. Atmospheric environment, 173, 127-141.

Godec, R., Jakovljević, I., Šega, K., Čačković, M., Bešlić, I., Davila, S. and Pehnec, G., 2016. Carbon species in PM_{10} particle fraction at different monitoring sites. Environmental pollution, 216, 700-710.

Górka, M., Kosztowniak, E., Lewandowska, A.U. and Widory, D., 2020. Carbon isotope compositions and TC/OC/EC levels in atmospheric PM_{10} from Lower Silesia (SW Poland): spatial variations, seasonality, sources and implications. Atmospheric Pollution Research, 11, 1099-1114.

Gray, H. A., G. R. Cass, J. J. Huntzicker, E. K. Heyerdahl and J. A. Rau, 1986. Characteristics of Atmospheric Organic and Elemental Carbon Particle Concentrations in Los Angeles. Environ. Sci. Technol., 20, 580-589.

Hallquist, M., Wenger, J.C., Baltensperger, U., Rudich, Y., Simpson, D., Claeys, M., Dommen, J., Donahue, N.M., George, C., Goldstein, A.H. and Hamilton, J.F., 2009. The formation, properties and impact of secondary organic aerosol: current and emerging issues. Atmospheric chemistry and physics, 9, 5155-5236.

Hama, S.M., Ma, N., Cordell, R.L., Kos, G.P., Wiedensohler, A. and Monks, P.S., 2017a. Lung deposited surface area in Leicester urban background site/UK: Sources and contribution of new particle formation. Atmospheric Environment, 151, 94-107.

Hama, S.M., Cordell, R.L., Kos, G.P., Weijers, E.P. and Monks, P.S., 2017b. Sub-micron particle number size distribution characteristics at two urban locations in Leicester. Atmospheric Research, 194, 1-16.

Hama, S.M.L., Cordell, R.L. and Monks, P.S., 2017c. Quantifying primary and secondary source contributions to ultrafine particles in the UK urban background. Atmospheric Environment, 166, 62-78.

Hama, S.M., Cordell, R.L., Staelens, J., Mooibroek, D. and Monks, P.S., 2018. Chemical composition and source identification of PM_{10} in five North Western European cities. Atmospheric research, 214, 135-149.

Harrison, R.M., 2020. Airborne particulate matter. Philosophical Transactions of the Royal Society A, 378, p.20190319.

Harrison, R., Jones, A., Lawrence, R., 2004. Major component composition of PM 10 and PM 2.5 from roadside and urban background sites. Atmos. Environ. 38, 4531–4538.

Ho, K., Lee, S., Chan, Ch., Yu, J., Chow, J., Yao, X., 2003. Characterization of chemical species in PM 2.5 and PM 10 aerosols in Hong Kong. Atmos. Environ. 37, 31–39.

Ho, K.F., Lee, S.C., Yu, J.C., Zou, S.C., Fung, K., 2002. Carbonaceous characteristics of atmospheric particulate matter in Hong Kong. Sci. Total Environ. 300, 59–67.

IPCC, 2014: Climate Change 2014: Synthesis Report. Contribution of Working Groups I, II and III to the Fifth Assessment Report of the Intergovernmental Panel on Climate Change [Core Writing Team, R.K. Pachauri and L.A. Meyer (eds.)]. IPCC, Geneva, Switzerland, 151 pp.

Janssen, N.A., Hoek, G., Simic-Lawson, M., Fischer, P., Van Bree, L., Ten Brink, H., Keuken, M., Atkinson, R.W., Anderson, H.R., Brunekreef, B. and Cassee, F.R., 2011. Black carbon as an additional indicator of the adverse health effects of airborne particles compared with PM_{10} and $PM_{2.5}$. Environmental health perspectives, 119, 1691-1699.

Ji, D., Zhang, J., He, J., Wang, X., Pang, B., Liu, Z., Wang, L. and Wang, Y., 2016. Characteristics of atmospheric organic and elemental carbon aerosols in urban Beijing, China. Atmospheric Environment, 125, 293-306.

Joaquin, 2015. Composition and source apportionment of PM_{10}. Joint Air Quality Initiative, Work Package 1 Action 2 and 3, Aalst, Flanders Environment Agency (2015). Available at Joaquin_WP1_PM_{10}_report_final_TW.pdf&rlz=1C1GCEB_enGB943GB943&oq=Joaquin_WP1_PM_{10}_report_final_TW.pdf&aqs=chrome.0.69i59l2j69i60.377j0j7&sourceid=chrome&ie=UTF-8.

Kelly, F.J. and Fussell, J.C., 2015. Air pollution and public health: emerging hazards and improved understanding of risk. Environmental geochemistry and health, 37, 631-649.

Kim, W., Lee, H., Kim, J., Jeong, U. and Kweon, J., 2012. Estimation of seasonal diurnal variations in primary and secondary organic carbon concentrations in the urban atmosphere: EC tracer and multiple regression approaches. Atmospheric environment, 56, 101-108.

Kim, Y., Yi, S.M. and Heo, J., 2020. Fifteen-year trends in carbon species and PM2.5 in Seoul, South Korea (2003–2017). Chemosphere, 261, 127750.

Kubelová, L., Vodička, P., Schwarz, J., Cusack, M., Makeš, O., Ondráček, J. and Ždímal, V., 2015. A study of summer and winter highly time-resolved submicron aerosol composition measured at a suburban site in Prague. Atmospheric Environment, 118, 45-57.

Lanz, V.A., Prévôt, A.S.H., Alfarra, M.R., Weimer, S., Mohr, C., DeCarlo, P.F., Gianini, M.F.D., Hueglin, C., Schneider, J., Favez, O. and d'Anna, B., 2010. Characterization of aerosol chemical composition with aerosol mass spectrometry in Central Europe: an overview. Atmospheric Chemistry and Physics, 10, 10453-10471.

Liao, W., Zhou, J., Zhu, S., Xiao, A., Li, K. and Schauer, J.J., 2020. Characterization of aerosol chemical composition and the reconstruction of light extinction coefficients during winter in Wuhan, China. Chemosphere, 241, 125033.

Lin, J., Tai, H., 2001. Concentrations and distributions of carbonaceous species in ambient particles in Kaohsiung City, Taiwan. Atmos. Environ. 35, 2627–2636.

Liu B., Bi X., Feng Y., Dai Q., Xiao Z., Li L., Wu J., Yuan J., Zhang Y., 2016. Fine carbonaceous aerosol characteristics at a megacity during the Chinese spring festival as given by OC/EC online measurements. Atmos Res 181:20 – 28.

Lu, Z., Streets, D., Winijkul, E., Yan, F., Chen, Y., Bond, T., Feng, Y., Dubey, M., Liu, Sh., Pinto, J., Carmichael, G., 2015. Light absorption properties and radiative effects of primary organic aerosol emissions. Environ. Sci. Technol. 49, 4868–4877.

Mancilla, Y., Herckes, P., Fraser, M., Mendoza, A., 2015. Secondary organic aerosol contributions to PM2.5 in Monterrey, Mexico: temporal and seasonal variation. Atmos. Res. 153, 348–359.

Mauderly, J.L. and Chow, J.C., 2008. Health effects of organic aerosols. Inhalation toxicology, 20, 257-288.

Mbengue, S., Fusek, M., Schwarz, J., Vodička, P., Šmejkalová, A.H. and Holoubek, I., 2018. Four years of highly time resolved measurements of elemental and organic carbon at a rural background site in Central Europe. Atmospheric Environment, 182, 335-346.

Mkoma, S.L., Maenhaut, W., Chi, X., Wang, W. and Raes, N., 2009. Characterisation of PM_{10} atmospheric aerosols for the wet season 2005 at two sites in East Africa. Atmospheric Environment, 43, 631-639.

Monks, P.S., Granier, C., Fuzzi, S., Stohl, A., Williams, M.L., Akimoto, H., Amann, M., Baklanov, A., Baltensperger, U., Bey, I. and Blake, N., 2009. Atmospheric composition change–global and regional air quality. Atmospheric environment, 43, 5268-5350.

Monteiro dos Santos, D., Brito, J., Godoy, J., Artaxo, P., 2016. Ambient concentrations and insights on organic and elemental carbon dynamics in Sao Paulo, Brazil. Atmos. Environ. 144, 226–233.

Mugica, V., Ortiz, E., Molina, L., de Vizcaya-Ruiz, A., Nebot, A., Quintana, R., Aguilar, J., Alcántara, E., 2009. PM composition and source reconciliation in Mexico City. Atmos. Environ. 43, 5068–5074.

Novakov, T., Menon, S., Kirchstetter, T., 2005. Aerosol organic carbon to black carbon ratios: analysis of published data and implications for climate forcing. J. Geophys. Res. Atmos. 110.

Noziere, B., Kalberer, M., Claeys, M., Allan, J., D'Anna, B., Decesari, S., Finessi, E., Glasius, M., Grgic, I., Hamilton, J.F. and Hoffmann, T., 2015. The molecular identification of organic compounds in the atmosphere: state of the art and challenges. Chemical reviews, 115, 3919-3983.

Pachauri, R.K., Allen, M.R., Barros, V.R., Broome, J., Cramer, W., Christ, R., Church, J.A., Clarke, L., Dahe, Q., Dasgupta, P. and Dubash, N.K., 2014. Climate change 2014: synthesis report. Contribution of Working Groups I, II and III to the fifth assessment report of the Intergovernmental Panel on Climate Change (p. 151). Ipcc.

Pandis, S.N., Harley, R.A., Cass, G.R. and Seinfeld, J.H., 1992. Secondary organic aerosol formation and transport. Atmospheric Environment. Part A. General Topics, 26, 2269-2282.

Pandolfi, M., Mooibroek, D., Hopke, P., Pinxteren, D.V., Querol, X., Herrmann, H., Alastuey, A., Favez, O., Hüglin, C., Perdrix, E. and Riffault, V., 2020. Long-range and local air pollution: what can we learn from chemical speciation of particulate matter at paired sites?. Atmospheric Chemistry and Physics, 20, 409-429.

Pani, S.K., Chantara, S., Khamkaew, C., Lee, C.T. and Lin, N.H., 2019. Biomass burning in the northern peninsular Southeast Asia: aerosol chemical profile and potential exposure. Atmospheric Research, 224, 180-195.

Panteliadis, P., Hafkenscheid, T., Cary, B., Diapouli, E., Fischer, A., Favez, O., Quincey, P., Viana, M., Hitzenberger, R., Vecchi, R. and Saraga, D., 2015. ECOC comparison exercise with identical thermal protocols after temperature offset correction–instrument diagnostics by in-depth evaluation of operational parameters. Atmospheric Measurement Techniques, 8, 779-792.

Peng, J., Hu, M., Gong, Z., Tian, X., Wang, M., Zheng, J., Guo, Q., Cao, W., Lv, W., Hu, W., Wu, Z., Guo, S., 2016. Evolution of secondary inorganic and organic aerosols during transport: a case study at a regional receptor site. Environ. Pollut. 218, 794–803.

Pérez, I.A., Artuso, F., Mahmud, M., Kulshrestha, U., Sánchez, M.L. and García, M., 2015. Applications of air mass trajectories. Advances in Meteorology, 2015.

Pio, C., Cerqueira, M., Harrison, R.M., Nunes, T., Mirante, F., Alves, C., Oliveira, C., de la Campa, A.S., Artíñano, B. and Matos, M., 2011. OC/EC ratio observations in Europe: Re-thinking the approach for apportionment between primary and secondary organic carbon. Atmospheric Environment, 45, 6121-6132.

Pipal, A.S. and Satsangi, P.G., 2015. Study of carbonaceous species, morphology and sources of fine ($PM_{2.5}$) and coarse (PM_{10}) particles along with their climatic nature in India. Atmospheric Research, 154, 103-115.

Pöschl, U., 2005. Atmospheric aerosols: composition, transformation, climate and health effects. Angewandte Chemie International Edition, 44, 7520-7540.

Ramana, M.V., Ramanathan, V., Feng, Y., Yoon, S.C., Kim, S.W., Carmichael, G.R. and Schauer, J.J., 2010. Warming influenced by the ratio of black carbon to sulphate and the black-carbon source. Nature Geoscience, 3, 542-545.

Ramachandran, S., Rengarajan, R. and Sarin, M.M., 2009. Atmospheric carbonaceous aerosols: issues, radiative forcing and climate impacts. Current Science, 97, 18-20.

Ramírez, O., de la Campa, A.S. and de la Rosa, J., 2018. Characteristics and temporal variations of organic and elemental carbon aerosols in a high–altitude, tropical Latin American megacity. Atmospheric Research, 210, 110-122.

Ramírez, O., de la Campa, A.S., Amato, F., Catacolí, R.A., Rojas, N.Y. and de la Rosa, J., 2018. Chemical composition and source apportionment of PM_{10} at an urban background site in a high–altitude Latin American megacity (Bogota, Colombia). Environmental Pollution, 233, 142-155.

Safai, P.D., Raju, M.P., Rao, P.S.P. and Pandithurai, G., 2014. Characterization of carbonaceous aerosols over the urban tropical location and a new approach to evaluate their climatic importance. Atmospheric environment, 92, 493-500.

Salma, I., Chi, X., Maenhaut, W., 2004. Elemental and organic carbon in urban canyon and background environments in Budapest, Hungary. Atmos. Environ. 38, 27–36.

Sánchez Campa De La, A., Pio, C., de la Rosa, J., Querol, X., Alastuey, A., González-Castanedo, Y., 2009. Characterization and origin of EC and OC particulate matter near the Doñana National Park (SW Spain). Environ. Res. 109, 671–681.

Schwarz, J., Chi, X., Maenhaut, W., Civiš, M., Hovorka, J., Smolík, J., 2008. Elemental and organic carbon in atmospheric aerosols at downtown and suburban sites in Prague. Atmos. Res. 90, 287–302.

Shivani, Gadi, R., Sharma, S.K. and Mandal, T.K., 2019. Seasonal variation, source apportionment and source attributed health risk of fine carbonaceous aerosols over National Capital Region, India. Chemosphere, 237, 124500.

Singh, R., Kulshrestha, M.J., Kumar, B. and Chandra, S., 2016. Impact of anthropogenic emissions and open biomass burning on carbonaceous aerosols in urban and rural environments of Indo-Gangetic Plain. Air Quality, Atmosphere & Health, 9, 809-822.

Sonwani, S. and Saxena, P., 2021. Water-insoluble carbonaceous components in rainwater over an urban background location in Northern India during pre-monsoon and monsoon seasons. Environmental Science and Pollution Research, 1-16.

Sonwani, S., Saxena, P. and Shukla, A., 2021. Carbonaceous aerosol characterization and their relationship with meteorological parameters during summer monsoon and winter monsoon at an industrial region in Delhi, India. Earth and Space Science, 8, 2020EA001303.

Stein, A.F., Draxler, R.R., Rolph, G.D., Stunder, B.J., Cohen, M.D. and Ngan, F., 2015. NOAA's HYSPLIT atmospheric transport and dispersion modeling system. Bulletin of the American Meteorological Society, 96, .2059-2077.

Stocker T. F. et al., Eds., "Intergovernmental panel on climate change" in Climate Change 2013: The Physical Science Basis. Contribution of Working Group I to the Fifth Assessment Report of the Intergovernmental Panel on Climate Change (Cambridge Univ Press, New York, 2013), 571–657

Terzi, E., Argyropoulos, G., Bougatioti, A., Mihalopoulos, N., Nikolaou, K. and Samara, C., 2010. Chemical composition and mass closure of ambient PM_{10} at urban sites. Atmospheric Environment, 44, 2231-2239.

Turpin, B.J. and Lim, H.J., 2001. Species contributions to PM2. 5 mass concentrations: Revisiting common assumptions for estimating organic mass. Aerosol Science & Technology, 35, 602-610.

Vargas, F., Rojas, N., Pachón, J., Russell, A., 2012. PM_{10} characterization and source apportionment at two residential areas in Bogota. Atmos. Pollut. Res. 3, 72–80.

Viana, M., Chi, X., Maenhaut, W., Cafmeyer, J., Querol, X., Alastuey, A., Mikuska, P., Vecera, Z., 2006. Influence of sampling artefacts on measured PM, OC and EC levels in carbonaceous aerosols in an urban area. Aerosol Sci. Technol. 40, 107–117.

Viana, M., Maenhaut, W., Chi, X., Querol, X. and Alastuey, A., 2007. Comparative chemical mass closure of fine and coarse aerosols at two sites in south and west Europe: implications for EU air pollution policies. Atmospheric Environment, 41, 315-326.

Vicente, E.D. and Alves, C.A., 2018. An overview of particulate emissions from residential biomass combustion. Atmospheric Research, 199, 159-185.

VMM, 2020. Vlaamse Milieumaatschappij Intra-Urban Variability Of Ultrafine Particles In Antwerp (February And October 2013). onlineAvailable at: <http://www.vmm.be> (accessed 21 February 2021).

Wang, Y., Khalizov, A., Levy, M. and Zhang, R., 2013. New Directions: Light absorbing aerosols and their atmospheric impacts. Atmospheric Environment, 81, 713-715.

Wang, Q., Jiang, N., Yin, S., Li, X., Yu, F., Guo, Y. and Zhang, R., 2017. Carbonaceous species in $PM_{2.5}$ and PM_{10} in urban area of Zhengzhou in China: Seasonal variations and source apportionment. Atmospheric Research, 191, 1-11.

WHO, 2016. World Health Organization: AAP Air Quality Database (2016) available at http://www.who.int/phe/health_topics/outdoorair/databases/cities/en/, (accessed 21 February 2021).

Wu, J., Bei, N., Hu, B., Liu, S., Wang, Y., Shen, Z., Li, X., Liu, L., Wang, R., Liu, Z. and Cao, J., 2020. Aerosol–photolysis interaction reduces particulate matter during wintertime haze events. Proceedings of the National Academy of Sciences, 117, .9755-9761.

Wyche, K.P., Cordell, R.L., Smallbone, K.L., Lyons, P., Hama, S.M.L., Monks, P.S., Staelens, J., Hofman, J., Stroobants, C., Roekens, E. and Kos, G.P.A., 2020. The spatio-temporal evolution of black carbon in the North-West European 'air pollution hotspot'. Atmospheric Environment, 243, 117874.

Xie, X., Chen, Y., Nie, D., Liu, Y., Liu, Y., Lei, R., Zhao, X., Li, H. and Ge, X., 2020. Light-absorbing and fluorescent properties of atmospheric brown carbon: A case study in Nanjing, China. Chemosphere, 251, 126350.

Yin, J., Harrison, R., 2008. Pragmatic mass closure study for PM 1.0, PM 2.5 and PM 10 at roadside, urban background and rural sites. Atmos. Environ. 42, 980–988

Yttri, K.E., Canonaco, F., Eckhardt, S., Evangeliou, N., Fiebig, M., Gundersen, H., Hjellbrekke, A.G., Lund Myhre, C., Platt, S.M., Prévôt, A.S. and Simpson, D., 2021. Trends, composition, and sources of carbonaceous aerosol at the Birkenes Observatory, northern Europe, 2001–2018. Atmospheric Chemistry and Physics, 21, 7149-7170.

Zhou, H., He, J., Zhao, B., Zhang, L., Fan, Q., Lü, Ch., Liu, T., Yuan, Y., 2016. The distribution of PM 10 and PM 2.5 carbonaceous aerosol in Baotou, China. Atmos. Res. 178:179, 102–113.

Zhang, Q., Worsnop, D.R., Canagaratna, M.R. and Jimenez, J.L., 2005. Hydrocarbon-like and oxygenated organic aerosols in Pittsburgh: insights into sources and processes of organic aerosols. Atmospheric Chemistry and Physics, 2005, 5, 3289-3311.

Zhang, H., McFarquhar, G.M., Cotton, W.R. and Deng, Y., 2009. Direct and indirect impacts of Saharan dust acting as cloud condensation nuclei on tropical cyclone eyewall development. Geophysical Research Letters, 36, L06802.

Supplementary Information

Table S1. Summarises the availability of meteorological data for each monitoring station. Ambient air temperature (T), Relative Humidity (RH) and Air Pressure (P), Radiation (RAD) and precipitation (PREC) were obtained from the nearest stations in the region.

Sites	Variables	Met station (distance, km)	Height (m)	Coordinates Latitude/Longitude
AD	T, RH, WS, WD, RAD, PREC	Schiphol (9)	30	52°18'39"N 4°46'12" E
AP	T, RH, WS, WD, RAD, PREC	Luchtbal (5)	30	51°15'40"N 4°25'28" E
LE	T, P, WS, WD, RAD, PREC	Groby road Traffic Island (4)	10	52°39'08"N, 1°10'34" W
LL	T, RH, P, WS, WD	Sequedin (7)	10	50°37'04"N 2°59'23" E
WZ	WS, WD	IJmuiden (4)	30	52°27'41"N 4°34'18" E

Table S2: Number of exposed filters used for gravimetric analysis of the PM_{10} mass concentration in all sites.

City	No of filter samples
Amsterdam (AD)	415
Antwerp (AP)	414

Leicester (LE)	388
Lille (LL)	328
Wijk aan Zee (WZ)	397
Total	1942

Section S1.

The EC/OC analysis was performed by GGD Amsterdam according to Technical Report CEN/TR16243 "Ambient air quality - guide for the measurement of elemental carbon (EC) and organic carbon (OC) deposited on filters". The analysis was done with a laboratory organic/elemental carbon aerosol analyser (Sunset Laboratory Inc, Tigard (OR), USA). The NIOSH protocol, which is most suitable for the traffic influenced PM_{10} samples of the Joaquin project, was selected for the analysis. The analytical parameters for the NIOSH protocol are given in Table S3. The OC analysis time is 360 s, the EC analysis time is 335 s.

Table S3. Temperature set points and plateau durations for NIOSH870 thermal protocol (min = minute; s= second).

Carrier gas	Time (s)	Total time	Temp (°C)
Purge time	10	10 s	
OC analysis			
Helium	80		310
Helium	80		475
Helium	80		615
Helium	110	6 min	870
EC analysis			

Helium	45		Oven cool
Oxygen in Helium	45		550
Oxygen in Helium	45		625
Oxygen in Helium	45		700
Oxygen in Helium	45		775
Oxygen in Helium	110	5 min and 35 s	890
Calibration	110	110 s	
Total	805	13 min and 25 s	

Table S4: Monthly average concentrations of all parameters measured and calculated at five cities.

Site	Months	PM_{10}	OC	EC	TC	OC/EC	OM	POC	SOC
AD	Jan	24.2 ± 15.3	3.81± 3.3	0.6 ± 0.18	4.4 ± 3.5	5.7± 3.5	5.3 ± 4.7	1.0 ± 0.2	2.7 ± 3.1
	Fev	15.4 ± 4.8	2.04± 0.7	0.52 ± 0.15	2.5 ± 0.8	3.95± 1.2	2.85 ± 1.07	0.9 ± 0.3	1.1 ± 0.6
	Mar	43.1 ± 15.5	4.36± 1.57	0.74± 0.23	5.0± 1.6	6.12± 2.3	6.1 ± 2.2	1.3 ± 0.4	3.0 ± 1.5
	Avr	38.6 ± 28.5	4.87 ± 4.3	0.64 ± 0.36	5.5 ± 4.5	7.1 ± 4.1	6.8 ± 5.9	1.1 ± 0.6	3.7± 3.5
	May	17.4 ± 4.7	2.3± 0.8	0.4± 0.09	2.7 ± 0.8	5.4± 2.2	3.2± 1.1	0.8± 0.1	1.5 ± 0.8
	Jun	21 ± 7.2	2.8 ± 1.2	0.5± 0.2	3.3± 1.5	5.1 ± 1.5	3.9 ± 1.7	0.9 ± 0.4	1.8± 0.9

	Jul	14.5 ± 3.5	3.0± 1.0	0.3 ± 0.1	3.4 ± 1.0	9.2 ± 4.2	4.2 ± 1.4	0.62± 0.1	2.4 ± 1.0
	Aug	19.4 ± 8.1	3.8 ± 1.53	0.45 ± 0.14	4.2± 1.6	8.4 ± 2.5	5.3 ± 2.1	0.8 ± 0.2	3.0 ± 1.4
	Sep	20.2 ± 9.8	2.8 ± 1.2	0.5± 0.2	3.4 ± 1.3	5.2± 2.1	3.9 ± 1.7	1.0 ± 0.3	1.8 ± 1.01
	Oct	14.9 ± 3.6	2.8± 0.9	0.7 ± 0.3	3.6 ± 1.0	4.1 ± 1.8	3.9 ± 1.2	1.3 ± 0.6	1.4± 1.0
	Nov	17.1 ± 5.1	2.1 ± 0.5	0.6 ± 0.3	2.8 ± 0.8	3.6 ± 1.1	3.0 ± 0.8	1.17± 0.5	0.9 ± 0.3
	Dec	22.5 ± 13.4	2.4 ± 0.8	0.83± 0.7	3.2 ± 1.5	3.7 ± 1.4	3.3 ± 1.1	1.4 ± 1.2	0.9 ± 0.6
AP	Jan	23.1 ± 8.7	3.8 ± 1.7	1.4 ± 0.3	5.3 ± 2.0	2.6 ± 1.0	5.3 ± 2.5	1.7 ± 0.4	2.1 ± 1.6
	Fev	19.1 ± 6.6	2.8 ± 1.0	1.5± 0.2	4.4± 1.1	1.8 ± 0.6	4.0 ± 1.4	1.7 ± 0.2	1.1 ± 0.9
	Mar	51.5 ± 22.0	6.8± 3.1	2.04± 1.2	8.8 ± 4.0	3.8 ± 1.9	9.5 ± 4.4	2.4 ± 1.4	4.4 ± 2.5
	Avr	44.7 ± 9.4	7.3± 1.9	2.0 ± 0.2	9.4 ± 2.0	5.4 ± 1.2	10.3 ± 2.7	2.4 ± 0.2	4.9 ± 1.8
	May	32.3 ± 16.1	2.7 ± 1.3	0.8 ± 0.5	3.5 ± 1.7	4.0 ± 1.6	3.9 ± 1.9	0.9 ± 0.5	1.8 ± 1.0
	Jun	22.5 ± 8.0	3.7 ± 1.8	1.1± 0.6	4.8 ± 2.3	3.3 ± 1.0	5.1 ± 2.5	1.38± 0.7	2.3 ± 1.3
	Jul	17.8 ± 4.1	3.77± 1.3	0.5± 0.14	4.3 ± 1.2	7.0 ± 3.8	5.2 ± 1.9	0.6 ± 0.1	3.0 ± 1.4
	Aug	23.5 ± 4.5	4.0± 1.7	1.5 ± 1.5	5.6 ± 3.2	2.7 ± 1.1	5.7 ± 2.4	1.7± 1.7	2.3 ± 0.4
	Sep	28 ± 17.8	3.82± 1.92	1.03 ± 0.29	4.8 ± 2.17	3.6 ± 1.15	5.35 ± 2.68	1.21 ± 0.34	2.6 ± 1.6
	Oct	23.4 ± 9.4	4.07± 1.2	1.89 ± 0.97	5.9 ± 1.93	2.49 ± 0.98	5.7 ± 1.68	2.22 ± 1.14	1.85 ± 1.08
	Nov	24.5 ± 16.3	3.5± 2.0	1.8± 1.1	5.4 ± 3.1	2.02 ± 0.39	4.99 ± 2.81	2.19 ± 1.4	1.38 ± 0.72
	Dec	27.6 ± 20.9	4.5 ± 3	2.2 ± 2.1	6.8 ± 5.1	2.4 ± 0.62	6.43 ± 4.2	2.63 ± 2.51	1.97 ± 0.78
LE	Jan	19.3 ± 12.12	4.45 ± 3.49	1.47 ± 1.65	5.9 ± 5.06	3.81 ± 1.86	6.23 ± 4.88	1.77 ± 1.98	2.68 ± 1.79

	Fev	11.2 ± 3.03	2.08 ± 0.66	0.76 ± 0.36	2.8 ± 1.0	3.01 ± 1.05	2.92 ± 0.93	0.91 ± 0.43	1.17 ± 0.34
	Mar	30.2 ± 16.23	4.41 ± 2.9	1.03 ± 0.7	5.4 ± 3.52	4.49 ± 1.8	6.18 ± 4.06	1.24 ± 0.85	3.18 ± 2.22
	Avr	26.7 ± 17.85	2.32 ± 1.09	0.52 ± 0.19	2.8 ± 1.25	4.56 ± 1.6	3.24 ± 1.53	0.62 ± 0.23	1.69 ± 0.92
	May	29.4 ± 6.07	5.26 ± 0.86	1.21 ± 0.15	6.4 ± 0.85	9.13 ± 2.01	7.36 ± 1.21	1.46 ± 0.18	3.8 ± 0.92
	Jun	14.8 ± 10.05	2.47 ± 0.85	0.5 ± 0.16	2.9 ± 0.98	5.06 ± 1.19	3.46 ± 1.19	0.61 ± 0.2	1.87 ± 0.73
	Jul	19.1 ± 7.98	4.84 ± 1.38	0.58 ± 0.05	5.4 ± 1.33	8.61 ± 2.99	6.78 ± 1.93	0.69 ± 0.07	4.15 ± 1.43
	Aug	12.9 ± 7.48	3.29 ± 1.15	0.85 ± 0.52	4.1 ± 1.33	5.03 ± 3.44	4.61 ± 1.62	1.02 ± 0.62	2.27 ± 1.23
	Sep	19.3 ± 13.99	3.41 ± 1.92	0.97 ± 0.33	4.3 ± 2.23	3.36 ± 1.02	4.78 ± 2.69	1.17 ± 0.39	2.24 ± 1.56
	Oct	10.1 ± 2.55	2.1 ± 0.39	0.79 ± 0.22	2.8 ± 0.58	2.76 ± 0.62	2.94 ± 0.54	0.95 ± 0.27	1.15 ± 0.25
	Nov	20.8 ± 12.05	3.64 ± 2.07	2.46 ± 2.17	6.1 ± 4.23	2.04 ± 1.02	5.1 ± 2.89	2.96 ± 2.61	0.69 ± 0.55
	Dec	13.1 ± 8.22	2.37 ± 1.66	0.86 ± 0.78	3.2 ± 2.43	3.2 ± 0.73	3.31 ± 2.33	1.03 ± 0.94	1.34 ± 0.78
LL	Jan	19.9 ± 6.27	4.18 ± 1.98	1.47 ± 0.67	5.6 ± 2.61	2.83 ± 0.6	5.85 ± 2.77	1.77 ± 0.8	2.41 ± 1.28
	Fev	12.1 ± 3.88	2.33 ± 0.83	0.88 ± 0.25	3.2 ± 1.04	2.66 ± 0.7	3.26 ± 1.16	1.06 ± 0.31	1.27 ± 0.63
	Mar	52.4 ± 25.14	7.34 ± 2.83	1.52 ± 0.72	8.8 ± 3.28	5.95 ± 4.99	10.27 ± 3.96	1.82 ± 0.86	5.51 ± 2.47
	Avr	32.6 ± 15.02	3.91 ± 1.99	0.95 ± 0.47	4.8 ± 2.27	4.42 ± 2.12	5.47 ± 2.78	1.15 ± 0.56	2.76 ± 1.75
	May	27.7 ± 17.16	3.02 ± 1.11	0.82 ± 0.26	3.8 ± 1.34	3.7 ± 1.1	4.23 ± 1.56	0.99 ± 0.31	2.03 ± 0.87

	Jun	28.9 ± 17.02	3.51 ± 1.33	0.91 ± 0.15	4.4 ± 1.43	3.79 ± 1.14	4.91 ± 1.86	1.1 ± 0.17	2.41 ± 1.21
	Jul	20.1 ± 5.76	4.25 ± 1.08	0.7 ± 0.2	4.9 ± 1.28	6.14 ± 0.24	5.95 ± 1.51	0.84 ± 0.24	3.41 ± 0.83
	Aug	24.6 ± 11.25	4.33 ± 0.87	0.82 ± 0.3	5.16± 1.0	5.68 ± 1.66	6.06 ± 1.21	0.99 ± 0.36	3.34 ± 0.83
	Sep	26.9 ± 19.02	4.29 ± 2.49	1.16 ± 0.94	5.4 ± 3.32	4.1 ± 1.64	6.01 ± 3.48	1.39 ± 1.13	2.9 ± 1.64
	Oct	18.1 ± 6.27	2.96 ± 1.16	1.27 ± 0.51	4.2 ± 1.58	2.41 ± 0.78	4.15 ± 1.62	1.53 ± 0.62	1.43 ± 0.81
	Nov	16.6 ± 8.81	2.44 ± 1.94	0.92 ± 0.76	3.3± 2.7	2.65 ± 0.24	4.27 ± 2.72	1.39 ± 0.92	1.66 ± 1.04
	Dec	21.1 ± 6.79	4.19 ± 1.99	1.61 ± 0.84	5.8 ± 2.69	2.85 ± 1.02	5.87 ± 2.79	1.94 ± 1.01	2.25 ± 1.38
WZ	Jan	34.1 ± 16.16	4.11 ± 3.22	0.99 ± 0.39	5.1 ± 3.28	4.76 ± 3.89	5.75 ± 4.51	1.19 ± 0.47	2.91 ± 3.2
	Fev	28.9 ± 2.34	2.49 ± 0.97	1.41 ± 0.57	3.9 ± 1.44	1.83 ± 0.46	3.49 ± 1.35	1.7 ± 0.69	0.8 ± 0.67
	Mar	44.8 ± 17.43	3.88 ± 1.8	1.08 ± 0.97	4.9 ± 2.35	4.62 ± 3.72	5.44 ± 2.52	1.3 ± 1.16	2.58 ± 1.71
	Avr	79.1 ± 41.58	6.99 ± 4.98	1.23 ± 1.02	8.2 ± 5.73	15.01 ± 8.12	9.78 ± 6.97	1.48 ± 1.23	5.51 ± 4.65
	May	31.5 ± 10.37	4.09 ± 1.9	0.64 ± 0.46	4.7 ± 2.21	16.19 ± 7.8	5.73 ± 2.65	0.77 ± 0.55	3.32 ± 1.6
	Jun	25.3 ± 8.81	2.49 ± 1.06	0.78 ± 0.85	3.2 ± 1.71	6.01 ± 3.85	3.48 ± 1.49	0.94 ± 1.03	1.55 ± 0.96
	Jul	16.1 ± 8.43	2.41 ± 1	0.32 ± 0.25	2.7 ± 1.19	10.52 ± 5.84	3.38 ± 1.4	0.39 ± 0.3	2.02 ± 0.81
	Aug	18.9 ± 3.6	3.38 ± 1.37	0.52 ± 0.2	3.9 ± 1.27	8.23 ± 6.47	4.73 ± 1.91	0.62 ± 0.24	2.76 ± 1.51
	Sep	18.9 ± 4.62	2.25 ± 0.78	0.41 ± 0.19	2.6 ± 0.95	5.81 ± 1.25	3.15 ± 1.09	0.49 ± 0.23	1.76 ± 0.6

	Oct	19.6 ± 6	1.74 ± 0.95	0.69 ± 0.67	2.4 ± 1.59	3.56 ± 1.7	2.44 ± 1.33	0.83 ± 0.81	0.91 ± 0.34
	Nov	19.1 ± 6.13	1.4 ± 0.42	0.41 ± 0.18	1.8 ± 0.49	3.87 ± 1.33	1.96 ± 0.58	0.49 ± 0.21	0.91 ± 0.42
	Dec	35.5 ± 4.66	2.54 ± 0.62	1.47 ± 0.68	4 .0± 1.19	2.03 ± 0.87	3.55 ± 0.87	1.76 ± 0.81	0.77 ± 0.59

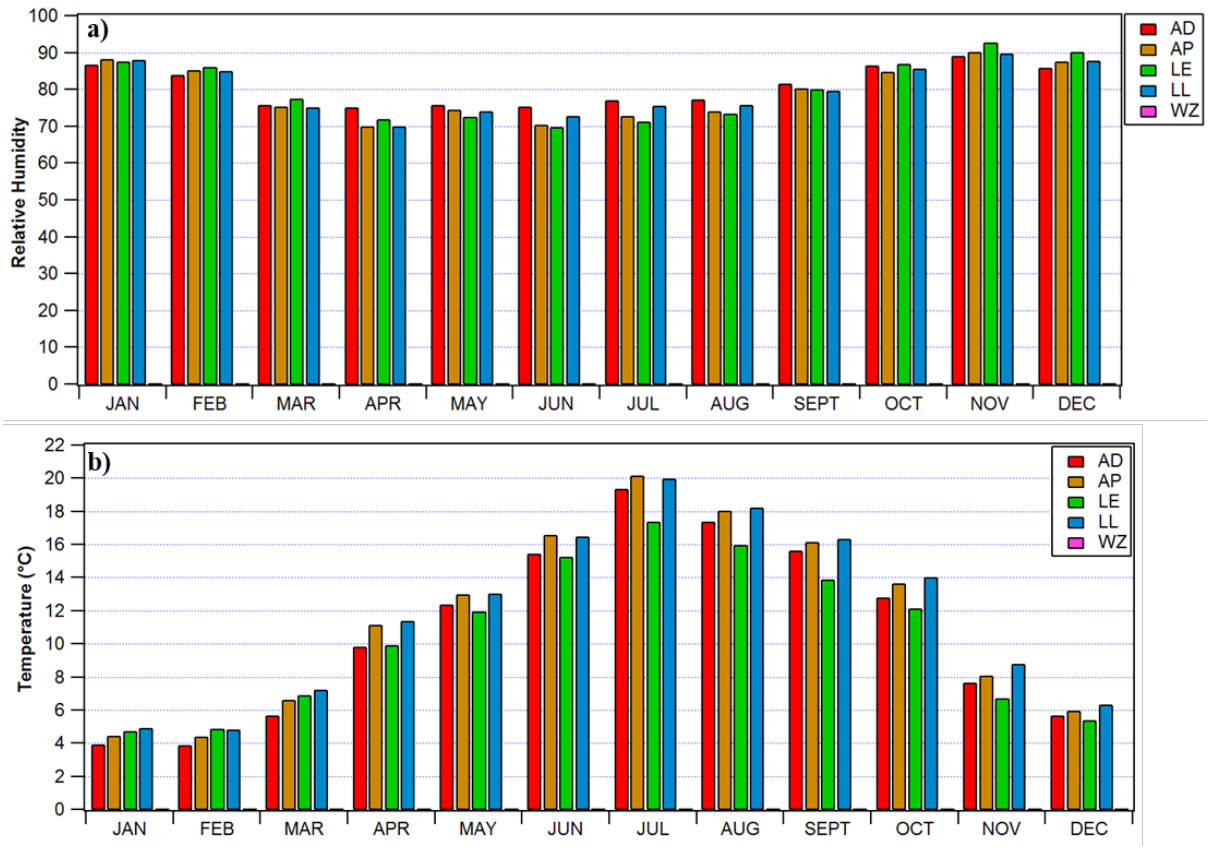

Figure S1. Monthly variation of the relative humidity (%) and temperature (ºC) during the study period in all sites.

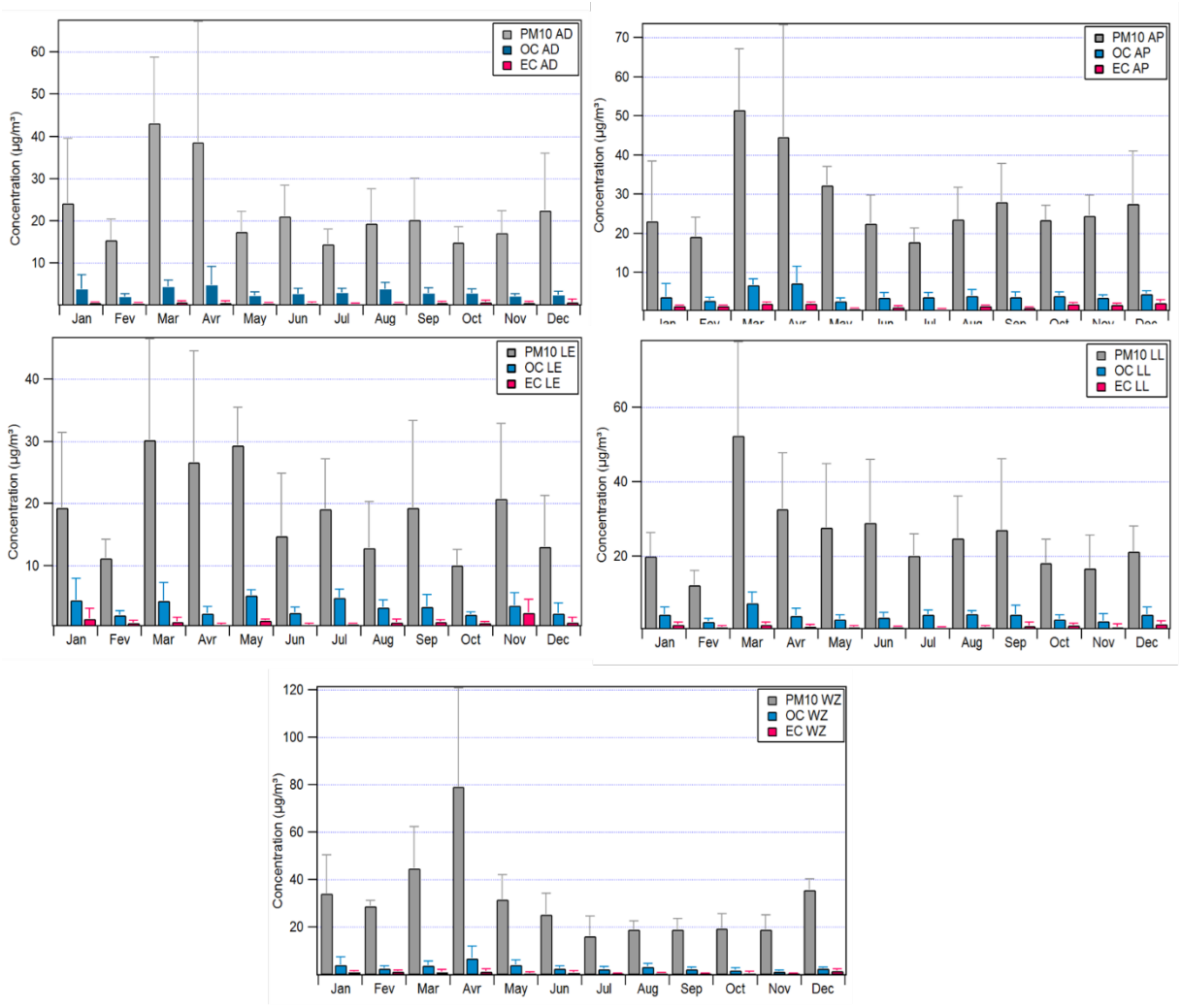

Figure S2. Monthly variation of PM_{10}, OC, and EC during the study period in Amsterdam, Antwerp, Leicester, Lille and Wijk aan Zee sites.

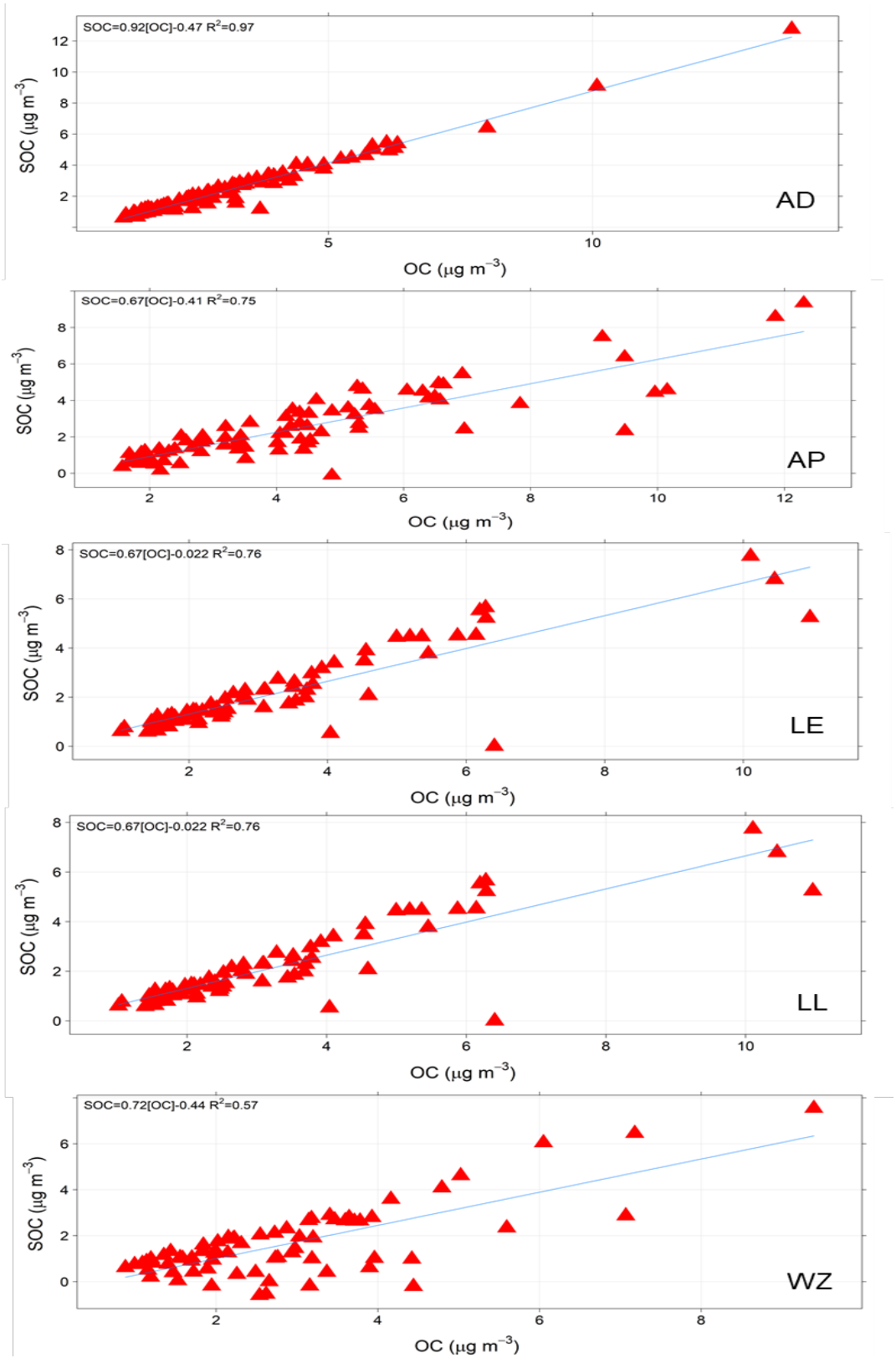

Figure S3. Correlation between SOC and OC for the five sites during the study period.

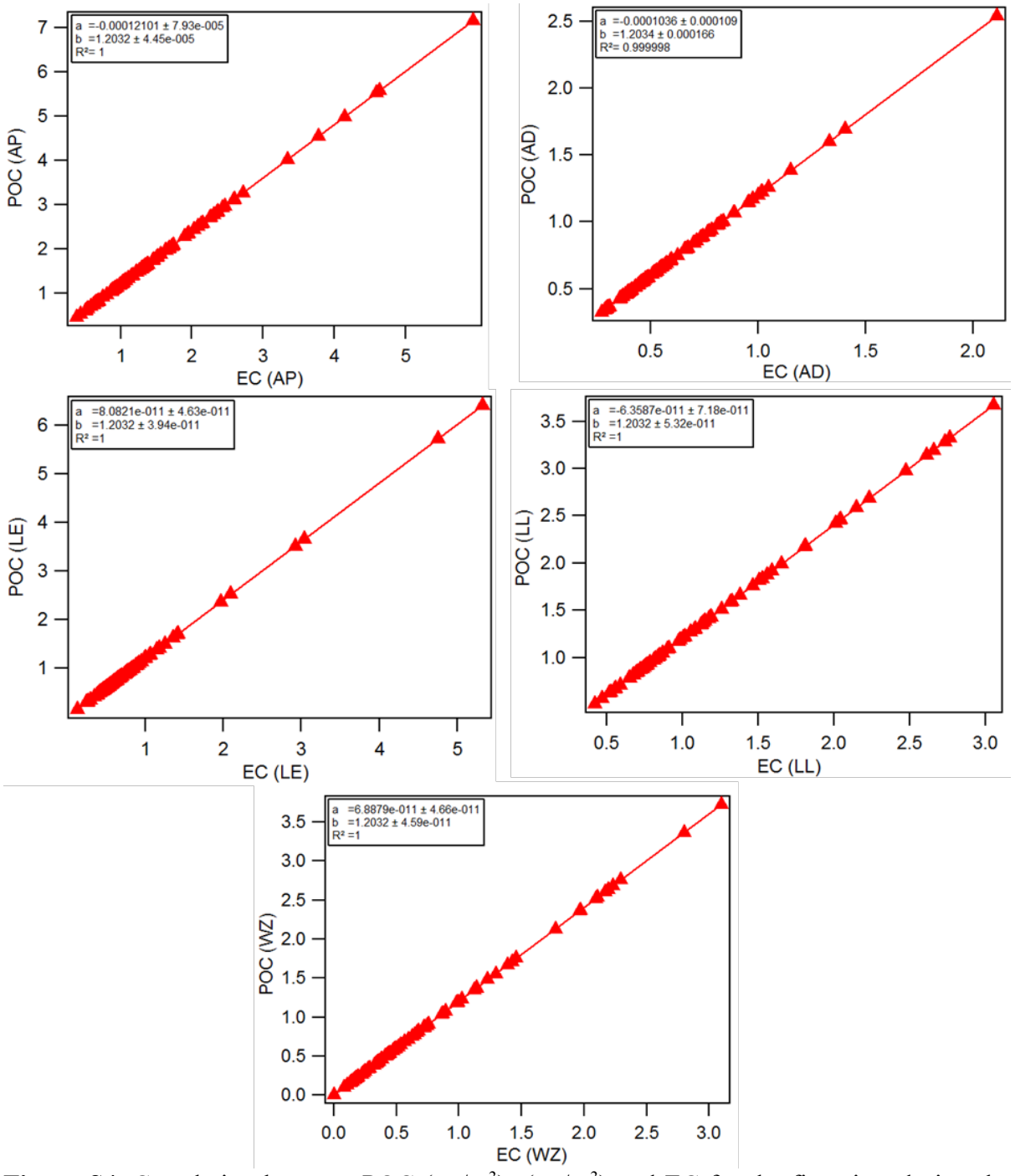

Figure S4. Correlation between POC (μg/m^3) (μg/m^3) and EC for the five sites during the study period.

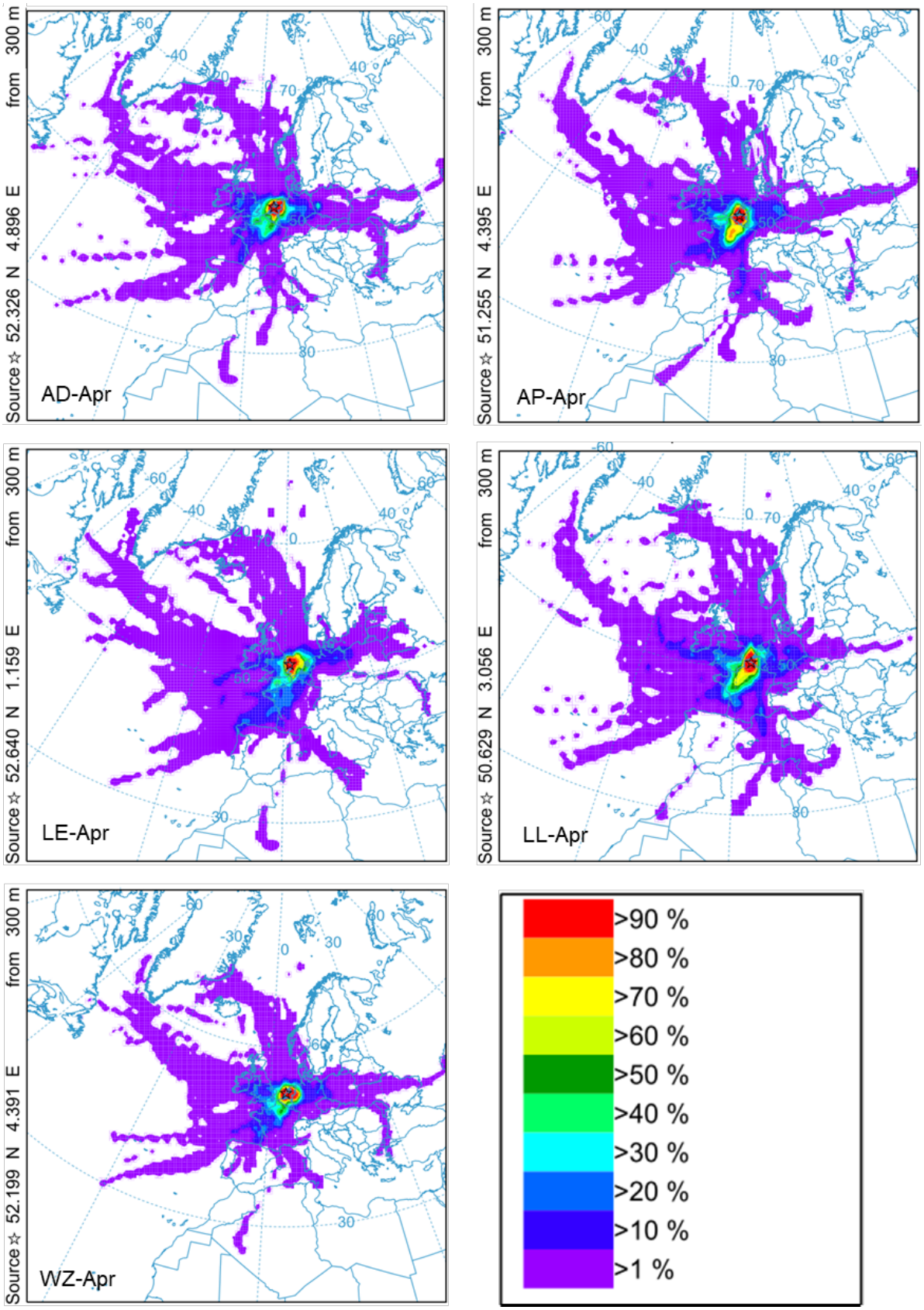

Figure S5. The backward trajectory frequency for the five studied sites at 300 m AGL, for April 2014, calculated by HYSPLIT Model.

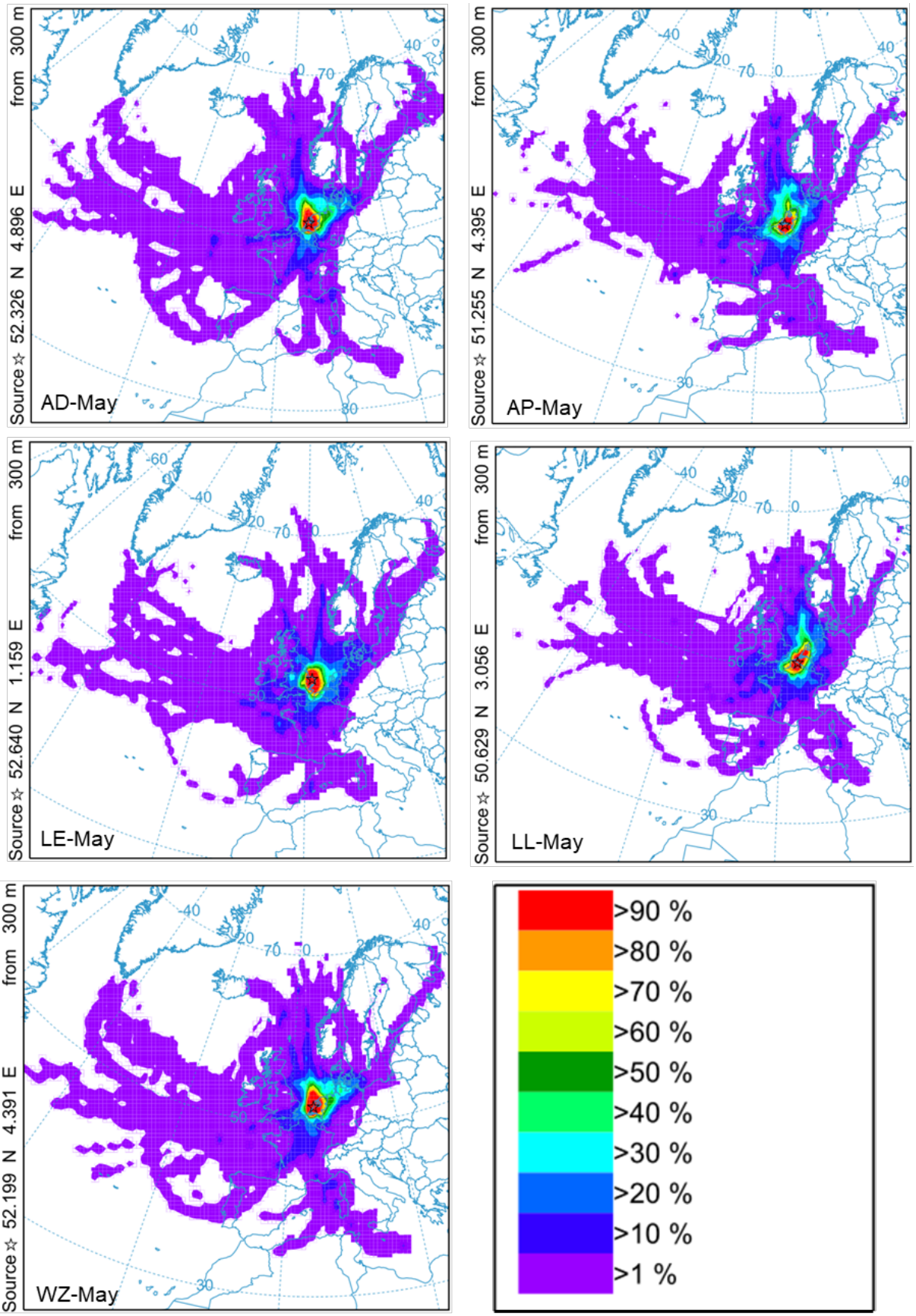

Figure S6. The backward trajectory frequency for the five studied sites at 300m AGL, for May 2014, calculated by HYSPLIT Model.

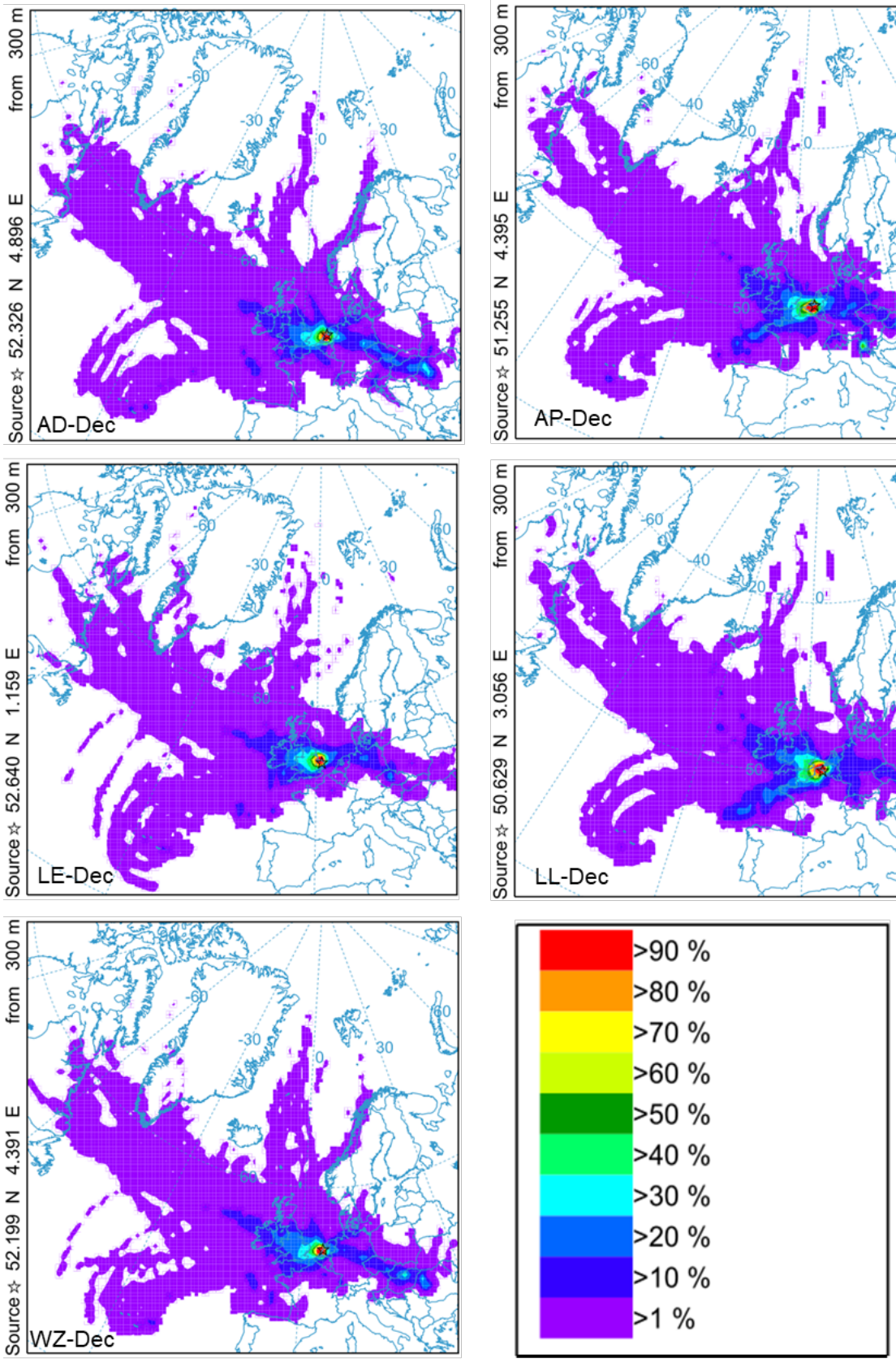

Figure S7. The backward trajectory frequency for the five studied sites at 300m AGL, for December 2014, calculated by the HYSPLIT Model.

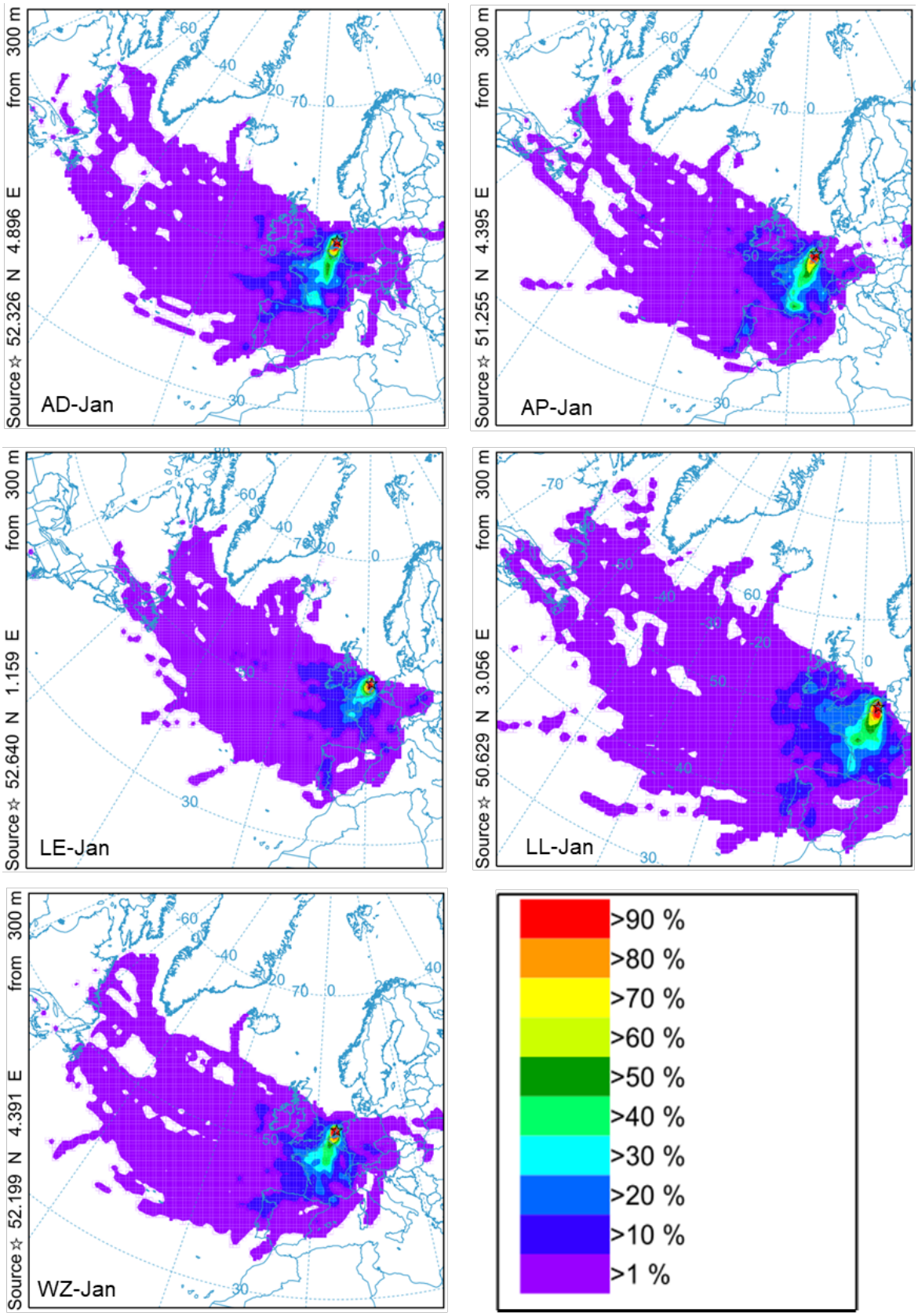

Figure S8. The backward trajectory frequency for the five studied sites at 300m AGL, for January 2014, calculated by the HYSPLIT Model.

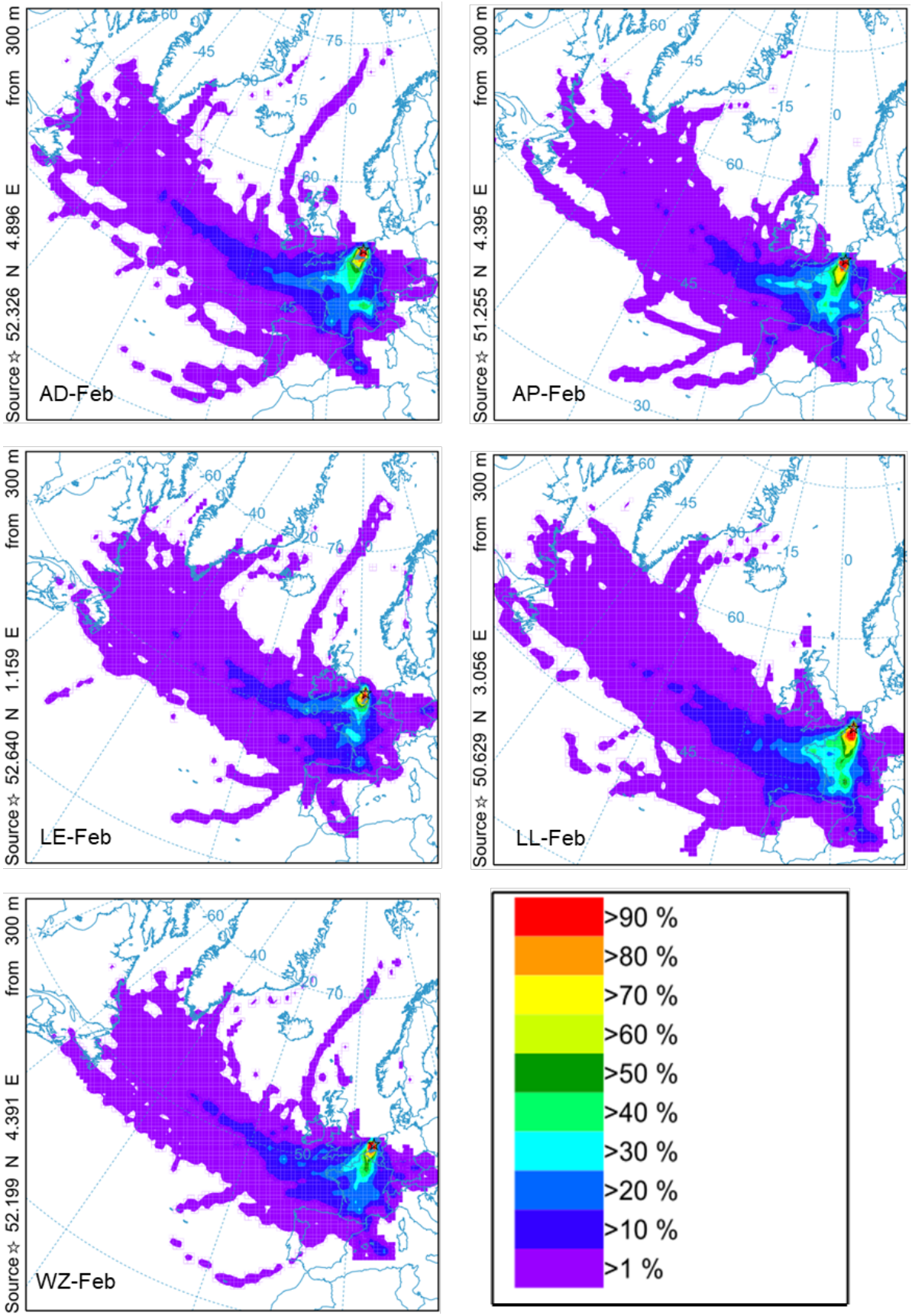

Figure S9. The backward trajectory frequency for the five studied sites at 300m AGL, for February 2014, calculated by the HYSPLIT Model.